Natural Hazards (2023) 116:3925–3955
https://doi.org/10.1007/s11069-023-05844-y

ORIGINAL PAPER

Simultaneous electric, magnetic and ULF anomalies associated with moderate earthquakes in Kumaun Himalaya

Jayashree Bulusu[1,2] · Kusumita Arora[1] · Shubham Singh[1] · Anusha Edara[1]

Received: 12 January 2022 / Accepted: 30 January 2023 / Published online: 2 March 2023

Abstract

Variations in electric and magnetic (EM) fields were examined at two sites: Dhanachuli near the Main Boundary Thrust (MBT) and Patiyasar near the Main Central Thrust (MCT) in Kumaun Himalaya, India. Anomalous EM signatures are defined based on medium-term data recordings. The patterns of anomalous EM signatures are then linked to the occurrence of moderate earthquakes ($3.5 \leq M \leq 5.0$), enhanced along the MCT. The vertical component of the magnetic field is due to microtremors prior to the earthquakes; electric fields also show positive anomalies. Surface waves due to microtemors associated with the earthquakes is reflected in the polarization ratios of geomagnetic data in the Pc4 range (0.01 Hz), a few days prior to each earthquake. In the case of one earthquake, during which suitable data could be retrieved, we observe a frequency change in ULF (Pc1 range) in addition to the enhancement of the Pc4, prior to the event.

Plain language summary

The search for EM precursors of earthquakes continues to be a promising one. In this pursuit, we have chosen a seismologically active region of Kumaun Himalaya and established geo-electromagnetic data acquisition systems. Scanning through about 5 months of data, we were able to detect anomalous variations in data through three independent approaches, which can be reliably ascribed to a seismogenic source. We present here the analysis of the patterns of these anomalous signals vis-à-vis the occurrences of about 15 earthquakes within a 250 km radius of our sites.

Keywords Electro-magnetic precursors · ULF waves · Geomagnetic pulsations · Moderate earthquakes

✉ Kusumita Arora
karora@ngri.res.in

[1] CSIR-National Geophysical Research Institute, Hyderabad, Telangana, India

[2] Indian Institute of Geomagnetism, Mumbai, India

1 Introduction

The overall long-term process of stress accumulation, particularly at plate boundaries, are at present relatively well known with the deployment of seismometers, GPS recorders and strain meters. But along the length of the plate boundary, there are spatial changes of fault geometry and frictional properties, fluid migration, rate of loading and strain accumulation. The latter two also change with time even at the same location, resulting in considerable variations in the patterns of seismicity at each location along the fault. Szakacs (2021) has verily explained that though seismogenic faults have several common general characteristics, each seismogenic fault has its specific tectonic setting, composition, structure, seismic history and stress field as well as relationships with contiguous structures. Moreover, earthquake occurrences are interlinked events; occurrence of one earthquake at a section of the plate boundary may increase or decrease the chances of occurrence of another in an adjacent section (Kanamori and Brodsky 2001). Thus, till today, much remains to be known about the short-term triggers, which vary vastly for each earthquake that produces the final failure. Hence, the prediction of the epicentral location, timing, magnitude and focal depth of an earthquake in the short- or long-term future appears to remain an impossible task (Jordan et al. 2011; Martinelli et al. 2020); indeed, a strong school of thought maintains that the highly sensitive nonlinear dependence makes prediction of earthquakes unviable (e.g. Geller et al. 1996; Geller 1997; Matthews 1997; Hough 2010). Even with so many different methods and different parameters recorded during different earthquakes, there has been controversial evidences that both negate and support the hypothesis of precursory signatures of earthquakes. While changes in dilatancy is considered as a probable mechanism, this process alone may not be sufficient. An integration of dilatancy–diffusion model with alternative models of earthquake generation process in which diffusion of fluids is not considered as the main factor—dry dilatancy models and stick–slip models are also essential while looking for precursory signatures (Bakhmutov and Groza 2008). The electric, magnetic and electromagnetic precursors deal with frequencies from Hz to MHz which also encompasses the frequencies caused by atmospheric noise from daily lightning (cloud-to-ground discharges) and flashes (cloud-to-cloud discharges) along the equilateral region. Lightening and flashes cause also vertically and horizontally polarized waves, respectively, which travel all around the earth through earth-ionosphere waveguides (Schumann resonances). It is extremely difficult, if not impossible, to distinguish local seismo-electromagnetic signals from these global effects even if the latter have been monitored for many decades. Other reported phenomena of preseismic geochemical fluids variations (groundwater level, vapour emissions, gases releases and radioactivity fluctuations) remain still ambiguous. This is because of the random distribution of the anomalies, which when correlated with the geographical system of seismic faults may be misleading, due to the randomness of earthquakes itself (Sorokin et al. 2020).

On the other hand, the efforts to achieve just this feat, with widely varying levels of success, have continued unabated from the 1960s to the present. As part of a priority program in Japan, systematic efforts to detect anomalies in foreshock activity, crustal deformation and geomagnetic changes were taken up five decades ago (Rikitake 1969). Similar efforts were made in the USSR Garm region and California, USA. Early estimates of earthquake occurrence time and precursor time were attempted based on the dilatancy model, which satisfied the Dambara–Utsu formula relating earthquake magnitude, foreshock area and area of crustal deformation and were supported by laboratory measurements and polarization anomalies in seismograms (Scholz et al. 1973; Rikitake 1975; Crampin et al. 1980).

Precursory observations in land as well as marine conditions of release of radon, methane, helium gases (Yasuoka et al. 2006; Pulinets and Boyarchuk 2005; Alam et al. 2020; Bella et al. 1995; Virk et al. 2001), fluctuations in groundwater levels (Chadha et al. 2006; Koizumi et al. 2004; Liu et al. 2006; De Santis et al. 2020 and many others), anomalous temperature variations (Ouzounov et al. 2007; Panda et al. 2007; Lu et al. 2016), acoustic-gravity wave oscillations (Molchanov et al. 2004a, b; Korepanov et al. 2009) have been explained by changes in dilatancy, fault dynamics, release of aerosols (Nikolaeva et al. 2009; Sorokin et al. 2020), variations in tidal force (Cochran et al. 2004; Tanaka et al. 2002). Ouzounov et al. (2018) and Wang et al. (2006) have demonstrated the viability of prediction based on precursors of several physical and environmental parameters, although repeatability of the predictions is not established.

The theories that support the atmospheric, electromagnetic precursor of earthquakes relate to the coupling of different regions of Earth. Research pursued by scientists in different parts of the world over the last three decades shows evidence for lithosphere-atmosphere–ionosphere coupling associated with physical processes prior to, during and after the eruption of an earthquake (Cieślik 2018; Main et al. 2012; Samuelson et al. 2009; Crampin et al. 1980). From the 1970s, investigations on detection of anomalous electric and magnetic signals associated with occurrence of earthquakes have gained strength. Park et al. (1993) have distinguished anomalies in the electric, magnetic and EM fields, suggesting the presence or absence of one or other points towards the causative mechanisms at play. Laboratory experiments establish that both resistivity and magnetization change when rocks are stressed, resistivity changes have also been recorded in active, and passive measurements in the field (Zhao et al. 1991) attributed to pore pressure changes. Variations in magnetic field amplitudes prior to earthquakes have been reported by many workers (Johnston et al. 1973, 1984), ascribed frequently to piezomagnetic effects due to stress removal. Effects of changes in pressure, temperature, grain size and dilatancy have been experimented with in laboratory scale experiments. Anomalous electric field enhancements have been reported from Japan and Greece (Varotzos and Alexopoulos 1986). Park (1996) have provided a review of electric signal precursors with or without corresponding magnetic signals and ascribed them to electrokinetic effect of fluid flow and transient electric fields. Fraser-Smith et al. (1990) observed increase in amplitudes of signals in the ULF bands 0.01–10 Hz as well as steady increase in noise levels prior to earthquake occurrence, perhaps induced by fluid flow at seismogenic depths. Dea et al. (1993) reported ULF signals at a ground observatory, correlatable to 29 M > 3.5 earthquakes over California and Nevada over an 18-month period but only with 7 of 67 M > 3.5 earthquakes in southern California within the same duration. These precursors could not be related to changes in stress–strain, measured in boreholes due to insufficient amplitudes of changes of the latter, but better correlation on the whole can be found with water level changes (Jin and Aki 1986). Such higher frequency changes have been attributed to piezoelectric effects (Warwick et al. 1982) or redistribution of electric charges (Gokhberg et al. 1982). Molchanov and Hayakawa (1998) developed a model of microfracturing and healing associated with rupture of a fault, which is capable of producing ULF emissions on the ground with upper cut-off of 1 Hz due to attenuation. ULF signatures have been identified to have occurred prior to many large earthquakes: Spitak earthquake $M=6.8$ (Kopytenko et al. 1993; Molchanov et al. 1992), Loma Prieta earthquake, $M=6.9$ (Fraser-Smith et al. 1990), Guam earthquake, $M=7.8$ (Hayakawa 1999; Kawate et al. 1998), Sumatra earthquake, $M=7.5$ (Ahadi et al. 2015), Tohuku earthquake, $M=9.1$ (Hayakawa et al. 2015), and Gorkha earthquake, $M=7.8$ (De Santis et al. 2017). Conti et al, (2021), have presented an exhaustive review of a large variety of ground-based precursory measurements and outcomes thereof; of the three different mechanisms suggested for generation of ULF precursors (magnetohydrodynamic, piezomagnetic and electrokinetic), the last is the most plausible one to explain the amplitudes of observed anomalies. Hayakawa and Fujinawa (1994) were one of the first to propose that seismic activity and neutral atmosphere oscillations lead to acoustic gravity waves (AGW), which in turn lead to anomalous ionospheric perturbations. The LAIC model of Pulinets and Ouzonov (2011) rests on the exhalation of radioactive gases to initiate conductivity changes in atmospheric layers inducing fluctuations of ionospheric parameters. Freund (2010) and Sorokin and Hayakawa (2014) proposed that stress build-up processes could give rise to an EMF near to the ground, which could cause ionospheric disturbances. Carbone et al. (2021) have developed a mathematical model for lithosphere–atmosphere–ionosphere coupling, which provides a quantitative basis to understand the mechanisms which modulate this complex system.

One model suggests that prior to an impending earthquake, charge separation within rock formations sets up streaming potential at the fluid–rock interface due to the relative differences of mass of electrons and ions, resulting in electromagnetic emissions which modify the local electric and magnetic fields (Chen et al. 2010; Han et al. 2009, 2014; Liu et al. 2006; Varotsos and Alexopoulos 1984a, b). Knowledge of the mechanisms by which the energies related to seismic and volcanic activities are converted to electromagnetic energies through electrokinetic, piezomagnetic, pressure stimulated currents, charge dislocation mechanisms or motional induction effects has advanced over the last decades based on laboratory experiments, field observations and theoretical developments (Eftaxias et al. 2002; Kapiris et al. 2003, 2004; Contoyiannis et al. 2005; Minadakis et al. 2012; Potirakis et al. 2012; Petraki et al. 2016; Gao et al. 2014). Surface waves associated with the process of microfracturing during the preparation phase of an earthquake propagate in the lithosphere and can bring changes in the vertical component of the magnetic field in the vicinity of the epicentral location before the actual earthquake event (Fujinawa et al. 2011). The LAIC model of Pulinets and Ouzonov (2011) is based primarily on the role of radon gas exhalations, released from a fault prior to its failure, which in turn would increase the local ionization in lower atmosphere causing a higher release of latent heat. Simultaneously, the conductivity of atmospheric layers would change affecting the Global Electric Circuit inducing fluctuations in the ionospheric parameters resulting in the formation of ionospheric irregularities, electromagnetic disturbances and the precipitation of charged trapped magnetospheric particles. The model includes a feedback process when precipitating electrons would increase the D layer ionization affecting: VLF reflection height, whistler dispersion, etc. More recently, Sorokin and Hayakawa (2014) proposed that preseismic processes would originate a current source near to ground that modify the lower atmosphere properties by generating an EMF (electro-motive force) that will cause ionospheric electromagnetic and plasma disturbances, a quasi-static electric field on ground and in space over the seismic region and the increase in conductivity with altitude. Associated with EMF enhancement, ionospheric instability can generate AGW, field-aligned currents and plasma irregularities along the magnetic tubes, spectral broadening of VLF transmitter signals, enhancement in space of ELF and changes in Schuman resonance harmonics. Such mechanisms are applicable both for in land and undersea earthquakes and are independent of the seismo-tectonic characteristics of the involved faults, as long as sufficient radon exhalation takes place.

With this current status of knowledge of earthquake and its association to EM signature, we venture to investigate the possible EM signatures in the northeast Himalayan range, which is one of the most active seismic zones of the world, with enormous potential of damage to the populous region in the Indo-Gangetic plains to its south. The 7.8 magnitude

Gorkha earthquake of 25 April 2015, which killed more than 9000 people along with devastating economical damage, is a recent reminder of the potential for earthquake hazard in this part of the world. The study area covers two of the important fault systems highly active in the Himalayan range: the Main Central Thrust (MCT) and the Main Boundary thrust (MBT). Both these fault systems are part of the lesser Himalaya. While the former describes the broad fault zone separating the Lesser Himalayan Domain (LHD) and Higher Himalayan Crystalline (HHC), the latter separates Proterozoic–Paleozoic rocks of the Lesser Himalayan Domain (LHD) from Tertiary foreland basin deposits of the Siwaliks. More details on the geology of the site are included in the subsequent sections (Figure A4 in Appendix).

We have selected an active region in the Kumaun Himalaya, which has the record of producing several small to moderate magnitude earthquakes every year and installed medium-term recording of magnetic and electric field variations. The continuous data provide the background regular variation in electromagnetic signatures, during quiet and active conditions of the magnetosphere, which allow us to identify anomalous signatures, which are not explained by magnetospheric/ionospheric sources. These anomalous variations in electric and magnetic fields are correlated with occurrences of medium and small magnitudes earthquakes in the vicinity (within 250 km radius) of the recording stations during the period of observation to study their correlation.

2 Data

Two stations are established in the eastern part of the Kumaun Himalaya at elevations of 2050 m MSL and 1940 m MSL. The southern station, Dhanachuli (DNC: geographic 29° 22′ 31″ N 79° 40′ 58″ E), is located 10 km north of the Main Boundary Thrust (MBT) while the second station Patiyasar (PTY: geographic: 30° N 79° E) is located 2.5 km north of the Main Central Thrust (MCT), depicted in Fig. 1. DNC was established first in September 2019, while PTY was commissioned in November 2019. Lemi 424/ flux gate magnetometer is used for magnetic field (1 s) and an induction coil magnetometer (64 Hz) used for magnetic field data collection. Porous pots are deployed to get the electric field measurements.

Fluxgate magnetic and horizontal electric field data from DNC are available over five months from mid-September 2019 to mid-February 2020, and induction coil data are available for one month; fluxgate magnetic and horizontal electric field data at PTY are available for two and half months from Dec 2019 to mid-February 2020. The remoteness of their locations imposes severe logistic constraints particularly in terms of power supply and accessibility, which have resulted in some data loss. On the other hand, the remoteness ensured anthropogenically undisturbed conditions, leading to generation of high-quality data. The line of our stations lies perpendicular to MBT and MCT, along the same geomagnetic longitude. We anticipated that the earthquakes would most likely cluster along the MCT; PTY could record possible small amplitude signatures associated with minor earthquakes. In case of moderate earthquakes, the relative amplitudes of the respective signatures at PTY and DNC would constrain the radius of detectability.

1 Hz data of horizontal electric field components E_x and E_y (10 µV/m sensitivity) and 1 Hz data of three components of geomagnetic variations (0.01 nT sensitivity) as well as 64 Hz band limited three component data from induction coils (0.001 nT) from the two sites have been analysed for this study. For the investigations of seismo-EM signatures,

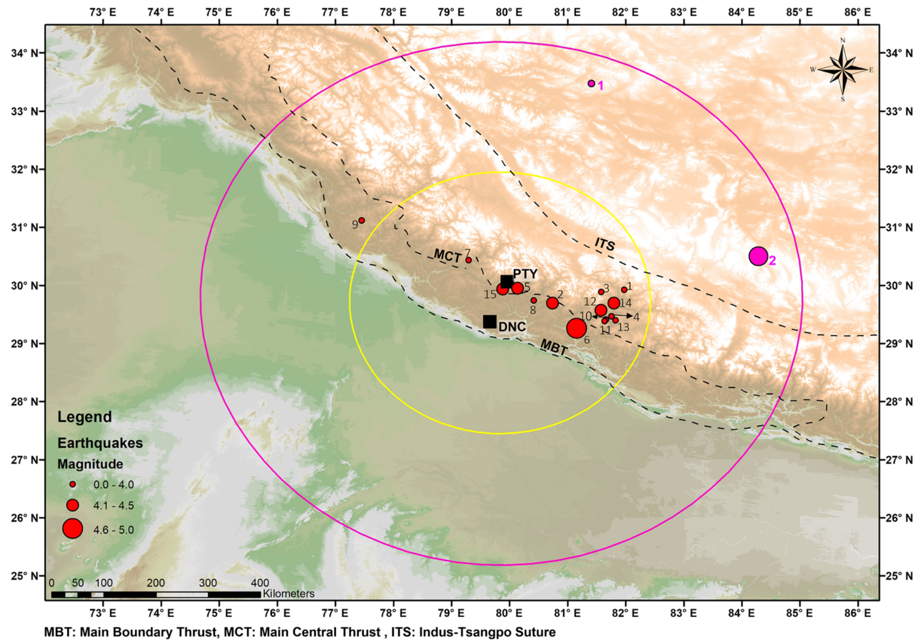

Fig. 1 Regional topographic map centred on Kumaun Himalaya, with geo-electromagnetic field stations DNC and PTY marked by black squares. Earthquake epicentres are marked by red dots. Two pink earthquakes represent the earthquakes in the radius of 300–500 km. The yellow and pink circles mark the 250 km and 500 km radius from the recording stations. The dashed lines mark the positions of MBT, MCT and Indus-Tsangpo Suture (ITS)

earthquakes of M ≥ 3.5, which occurred at shallow depths (< 20 km) and within 250 km radius of our stations and M ≥ 4.0 in a radius of 500 km from the sites (ISC catalogue; http://www.isc.ac.uk/), have been considered for the duration 14 Sept 2019 to 21 Feb 2020 (Table A1 in Appendix). The EM data and description for the period of investigation are presented in Figure A1 in Appendix.

3 Approach adopted

In order to define an anomaly in the geomagnetic and electric field signatures linked to earthquake, it is essential to infer the contributions of different source regions like lithosphere, atmosphere and ionosphere to the geomagnetic field. While the contributions from lithospheric conductivity and underneath subsurface geology have a dominant role in affecting the vertical component of magnetic field, the ionospheric currents and atmospheric wind pattern can result in changes in the *H* component at a given site. Hence, we define the anomaly in the electric and magnetic field by adopting certain procedures as briefly mentioned below and discussed in details in the subsections: (1) anomalous electric and magnetic field estimates are identified by quantitatively evaluating the contributions of solar origin to the geomagnetic *H* and *Z* components. The solar contributions are then removed from the observed electric and magnetic field to obtain the anomaly amplitude (see Sect. 4.1 for more details). (2) Evaluating the patterns of night time Pc4 (geomagnetic field variations in 7–22 mHz) patterns which are observed in both the vertical and horizontal components of the magnetic field. This particular band of ULF wave is sensitive to the lithosphere-atmosphere–ionosphere coupling (Yumoto et al. 2009). These Pc4s may not be driven by solar origin which are dominant in the day time and almost sparse in the night time in the latitudinal region of current study (Bulusu et al. 2020). Thus, an anomaly in Pc4 is considered when the Pc4 exists in both vertical and one of the horizontal components and its amplitude lies above the day time median value (see sub-Sect. 4.2 for more details). (3) We then examined the inter-linked patterns of all the anomalous signatures by superimposing the anomalies on the temporally recorded earthquakes from the beginning of data recording. The observation sites are located in same longitude; this allows us to compare the signatures of anomalies in the electric, magnetic and Pc4 polarization estimates and possibly link them to the underlying physics.

3.1 Anomalous electric and magnetic field signatures

The electric and magnetic field perturbations observed on the ground have contributions from both upper forcing from solar origin and lower forcing due to lithospheric origin. In order to define the anomalous electric and magnetic fields, the effect of solar forcing needs to be removed. For this purpose, we consider two methods. As a first step, the anomalies of observed electromagnetic signatures are made with comparison with global geomagnetic activity indices like planetary index *Kp*, geomagnetic storm time index *Dst* and the deviation from International quiet (IQ) and International disturbed (ID) days. These derived indices are globally accepted as a measure of the activity induces by solar forcing. As a second step, we compare the signatures of magnetic *Z* field from a reference site Jaipur (located in the similar latitude) to rule out the possibility of solar forcing. Based on the monthly mean of the electric field variation and standard deviation, a deviation of $\geq \pm 1$ mV/m with respect to average values of IQ and ID days, persistent over a minimum period of 2 h, was identified as anomaly in electric field. This criterion is applied to remove effects of artificial noise as well as be correlatable with variations in magnetospheric conditions in terms of ΣKp (mean of *Kp* over a day defined by WDC Kyoto) and *Dst*. With similar reasoning, all enhancements of the hourly mean of the *Z* component in the order of ± 5 nT of the magnetic field from the regular diurnal, which do not correspond to depressions in the *H* component and persist for a minimum of 2 h are identified as anomalous, possibly linked to lithospheric/seismic sources.

For example, the anomalous signatures of electric (E_x and E_y) and magnetic field (Z) for 14–30 September 2019 at DNC are shown in Fig. 2a–d. The black dashed lines (on 18 September 2019 and 22 September 2019) mark the days with anomalous fluctuations, which show departure from the regular IQ and ID trends of E_x, E_y and Z. The first increase is seen in E_y component during 14 September 2019, with no substantial signatures in E_x and Z. On 18 September 2019, there are impulsive changes in magnitudes of E_x, E_y and Z, which is similar to that on 22 September 2019, where *Z* departure is of larger magnitude. Neither on 18 September, nor on 22 September were there any depressions in H, also verified by trends of *Dst* and K_p.

3.2 Night time Pc4 patterns

Ultra-low-frequency waves or geomagnetic oscillations, or ULF pulsations as they are also called, have frequencies in the range 1 mHz–5 Hz and appear as more or less regular oscillations in records of the geomagnetic field. These waves can be identified in electric field measurements in the ionosphere as well as observations of the electromagnetic field of the magnetosphere as made onboard spacecraft. Oscillations with quasisinusoidal waveform are called pulsations continuous (Pc). Pc4s in particular lie in the frequency range of 7–25 mHz, driven by magnetospheric processes, are observed commonly during the day in the horizontal component of the magnetic field and are abundant during day time (Bulusu et al. 2020). Such events do not occur at night-time, nor are expressed in all three components. The other extreme frequency of geomagnetic pulsation is the Pc1 pulsation with frequencies ranging till 5 Hz and is abundant in the night side at a low latitude station.

We scan our data for night-time Pc4 events, which have expression in the vertical component along with in either one or both horizontal components, based on the hypothesis that the Pc4s seen in *Z* component will be driven by lithospheric processes (Yumoto et al. 2009). According to this hypothesis, the third model for the generation mechanism of ULF (aside from ULF emission) is the changing of geo-electric conductivity in the lithosphere at the EQ focal zone. According to the low-frequency magnetic field precursor model of Karakelian et al. (2000), the external EM waves impinging on a thin infinitely long wire with incident electric field parallel to the wire induce a current within the wire, which acts as an antenna and in turn creates a circumferential magnetic field. If the wire is thin compared to the external wavelength, we could expect high magnetic fields. Based on this mechanism, if a highly conductive long thin region was created under or nearly under the magnetometer towards the time of the earthquake, then the incident EM waves would have induced a high current in this region, which would create the anomalous high magnetic fields. Therefore, the conductive fault zone acts as an antenna to couple with the external EM field to generate the observed magnetic anomalies.

Hence, we have extracted the pulsations for which identical peak frequency of 10 ± 3 mHz is detected in the horizontal and vertical components. The amplitudes of these peaks are compared using polarization estimates (*Z*/*G* and *Z*/*H*, where $G = \sqrt{(H^2 + D^2)}$). It is evident that during daytime the ratio would be maximum because of the induction effect that results from Sq current and can increase the amplitude of Pc4 in *Z* as compared to the night time values. Thus, in order to nullify the effect of the ionospheric Sq current, only those values of polarizations are considered which lie above the median of daytime values as showcased below. The anomalous polarization estimates are influenced by site location and may not always be unity as has been proposed earlier (Hayakawa et al. 1999). Unambiguously detected anomalous Pc4s, as per above criteria, are attributable to lithospheric sources based on the geoelectric anomaly model of Yumoto et al. (2009).

The typical values of polarization estimates of *Z*/*G* are presented in Fig. 3a for the period of 14–30 September 2019. It is seen that *Z*/*G* varies between 0.2 and 1.2 during the 14–30 September 2019, and frequently clusters around 0.3. The day time median values are around 0.5, which may be the result of induction effect due to Sq currents. We adopt the approach that estimates of *Z*/*G*, which lie above the median values are anomalous. The typical Pc4 frequencies in three geomagnetic field components identified using spectrogram on 22 September 2019 are shown in Fig. 3b–d, respectively, illustrated in the rectangles. Thus, the anomalous polarization estimates are considered only if they are above the median of the polarization ratios (Figure A2 in Appendix).

3.3 Correlation with earthquake occurrences

Once the above-mentioned anomalous signatures are identified, we superpose the recorded earthquakes of $M \geq 3.5$, on the time series only. It should be noted that for deriving the comparison between anomaly pattern and earthquakes, the locations of earthquakes are assumed to be in the same space. We then qualitatively analyse the time correspondence and magnitudes of the anomalous signatures seen in E_x, E_y and Z as well as Z/G with respect to the earthquake occurrence to investigate whether consistent patterns exist. At this stage, it is not our objective to match precursors to each earthquake. Rather, the aim is to investigate the patterns of anomalous EM signatures from ground data, which are observed in a seismic zone and are absent at aseismic locations. When a section of lithosphere is undergoing deformation to successively generate moderate earthquakes within a relatively narrow frame of time, pre-quake EM signatures of one could very likely overlap with post-quake signatures of another. Pre-quake EM signatures could be generated by multiple earthquakes, thus making it complicated to assign to a particular seismic event. If robust signatures exist, it would contribute to design of early warning systems, which could save life and property.

3.4 Observation of anomalous Pc1

Gravity and acoustic wave frequencies higher than the acoustic cut-off frequency of 3.3 mHz, can reach up to the ionosphere (Astafyeva 2019), bringing an alteration to the electron and ion densities. This is reflected in both TEC variation. In addition, it is known that the acoustic waves caused by the surface displacement during seismic activity can reach up to the ionosphere, but they may not necessarily have an EM component. Hence although these waves do not alter the frequency of Pc1 waves, they can bring change in morphology and amplitude of these waves in the ionosphere due to the changes in the densities in the ionosphere. This may lead to alteration of incoming Pc1 structure (see Bortnik et al. 2008), creating an abrupt change in the usual pearl type variation. We examine our 64 Hz data to identify the altered Pc1 pulsations, in conjunction with the above-mentioned anomalous signals to provide additional evidence of lithospheric–ionospheric coupling associated with occurrence of earthquakes.

4 Results

4.1 Local conductivity structure

The northern site PTY is located on the slopes of the Higher Himalayan crystallines at 2040 m elevation with the folded cover sequence to the south. The terrain consists of volcano-sedimentary sequences that has been subjected to intense deformation and metamorphism up to amphibolite facies. The mafic volcanics are predominantly basalts, and the sedimentary unit consists of interbedded sequence of quartzites and phyllites. The basement gneisses that are exposed at the site exhibit a foliation N25W. During site setup processes, it was found that ground water is very shallow; where it intersects topography, a waterfall is formed about 100 m away. The site is prepared in several flat steps, each of which accommodates one set of sensors, maintaining a minimum distance of 30 m between each. The electrode separation is approximately 20 m.

The southern site DNC at a slightly lower altitude of 1940 m MSL consists predominantly of deformed granite gneisses overlain by felsic metavolcanics rocks with interbedded units of quartz–chlorite–schist. As the ground conductivity is an important parameter which facilitates/impedes the propagation of weak electromagnetic signatures perhaps generated due to earthquake preparation processes, we probe the ground conductivity at the two sites on the basis of impedance tensors. Estimates of tipper magnitudes, induction arrows and apparent resistivity are shown for DNC and for PTY in Fig. 4.

At DNC, the real parts of the tipper range from − 0.4 to 0.2 with minimum values at shorter periods which increase with longer periods as shown in Fig. 4a. This shows that the conductivity contrast within the penetrated volume increases with period. According to the Parkinson convention of induction arrows (Fig. 4b), it shows that for shorter periods the real induction vectors point towards N-E and rotates towards east up to 1200 s. For longer periods, the real vectors point to the N-W direction. The characteristic period at DNC is about 2880 s, where the magnitude of real component is maximum and the imaginary component shows a reversal of direction. The 1D model based on the apparent resistivity indicates a three-layered structure with a moderate conductive layer 120 Ωm at 8–25 km depth, then followed by resistive block of 2000 Ωm at 25–80 km depth and a highly conductive block at greater depths (Fig. 4c).

At PTY, the real parts of the tipper range from − 0.5 to − 0.2 with minimum values at smaller periods which increases with longer periods (with largest amplitude of 0.5) as shown in Fig. 4c (top). This shows that the conductivity contrast within the penetrated volume increases with period. The Parkinson convention induction arrows (Fig. 4c (bottom)) show that for shorter periods the real induction vectors point towards N-E up to 480 s. For longer periods, the real vectors point to the north. The characteristic period at PTY is observed at 2040s, where the magnitude of real induction arrow is maximum and the imaginary arrow has a very small amplitude, and the direction gets reversed. This represents the strongest conductivity contrast in the penetrated volume (Dosso and Chen 2000; Samrock and Kuvshinov 2013). The 1-D conductivity model shows a 2-layered structure with a resistivity of 400 Ωm at shallow depth of 30 km, followed by a resistive block of 12,000 Ωm at PTY as shown in Fig. 4d. Below 170 km, the layer regains the similar conductivity as of top layers. For both the sites, the induction arrows point to the north east for shorter periods and then turn north–south. The characteristic period increases from PTY to DNC, suggesting a higher conductivity contrast at greater depths at DNC, which can be linked to the outcrops of volcanics in the vicinity (Chamyal et al. 1989).

4.2 Anomalous electric and magnetic field signatures

Figure 5 shows the illustration of all the anomalous signatures identified according to our criteria in different datasets for current duration of observation. Panels (a) and (b) show the E_x and E_y data of both DNC and PTY. In E_x, twenty one anomalies are seen in five and a half months of DNC data with amplitudes ranges of 1–5 mV/m; eleven anomalies are seen in two and half months of PTY data, with amplitude ranges of 1–2 mV/m with one anomaly to the tune of 11 mV/m. For the duration of overlapping data, the number of anomalies is comparable. In E_y, fourteen anomalies at DNC are observed, with amplitude ranges of 1–20 mV/m; at PTY seven anomalies are identified with amplitudes 1–2 mV/m, with one anomaly of 13 mV/m corresponding to the enhanced amplitude of E_x. At both DNC and PTY, the E_y anomalies occur simultaneously to the corresponding E_x anomalies; some E_x anomalies do not exhibit the corresponding E_y anomaly. For the duration of concurrent data, we observe that anomalies interchangeably occur first either at DNC or at PTY with a 24 h lag/lead at the other station.

Panels (c) and (d) depict the anomalous signatures in *Z* component of DNC and PTY, respectively. Based on the patterns observed, we have segregated the anomalies as 'clusters' (successive anomalies over a duration of 24–48 h) and 'singulars' (individual standalone signatures). At DNC, eight clusters are observed of amplitudes 5–10 nT and seven singulars of comparable amplitudes. At PTY, four clusters of 5–10 nT and two singulars with lower amplitudes are observed. For the duration of simultaneous data, over December to mid-January, the patterns are observed as cluster-singular pairs over the two stations with same occurrence time. From mid-January to the end of the time series, singulars are seen at PTY, not observed at DNC. Around 15–20 February, a cluster is seen occurring at the same time at both stations.

4.3 Night-time Pc4 patterns

Anomalous polarization ratios of night-time Pc4s from DNC and PTY are shown in panels (e) and (f) of Fig. 5, respectively, for values higher than the day time maximum value of *Z*/*G*. At DNC, fifteen clusters are observed and eight singulars, at PTY ten clusters and three singulars. For the overlapping data, the numbers of clusters and singulars are similar at the two sites with some variations in the times of occurrences. The clusters and singulars of *Z*/*G* at both DNC and PTY have only partial time correspondence with the occurrence patterns of *Z* anomalies at the same location.

The comparison of data at PTY and DNC shows that the amplitudes of background as well as anomalous signatures in E_x, E_y, *Z* and *Z*/*G* at DNC and PTY are mostly consistent with each other. The electric fields at DNC have higher amplitude (30 times) than that at PTY, commensurate with higher conductivity below the site. In a similar manner, the *Z* component at DNC is higher (40 times) than that at PTY, explained by the strong induction component at the former. Hence, the anomaly amplitude in *Z* is higher at DNC. But the occurrence of *Z* anomalies is significantly more in number at PTY for the duration of concurrent measurements. As would be expected, the *Z*/*G* anomalies at DNC are about 1.5 times higher than that at PTY. As the *Z*/*G* anomalies are computed from seconds data, whereas the *Z* anomalies have been represented by hourly means, many singulars of the latter are reflected as clusters in the former.

4.4 Correlation of anomalies in electric, magnetic and polarization ratio with Earthquakes

The observed anomalies in E_x, E_y, *Z* and *Z*/*G* at DNC and PTY are correlated with the earthquakes which occurred during the recording period. A total of 15 earthquakes occurred during the period of investigation with magnitude of 3.5–5.0 (Fig. 5g), out of which 4 earthquakes occurred on 12 Jan 2020. A total of 12 earthquakes occurred within 250 km distance from recording site, and one earthquake at 285 km. There are two more earthquakes with magnitude of 4.2 and 4.6 approximately at 400 km from the recording sites.

The seismicity in the region is within the folded cover sequence about 55 km to the east and northeast of the stations and also to the northwest in the crystalline formations about 90–160 km away (Dasgupta et al. 2000). The anomalous signatures are correlated with the distance, magnitude and azimuthal directions of earthquakes from recording sites to understand the inter-relations between EM signals and lithospheric sources.

From the beginning of the recording period, there was enhancement in both *Z* and *Z*/*G* at DNC on 14 and 16 September 2019 without any corresponding signature in the E_x and E_y components at DNC. Two earthquakes of magnitudes 4 and 4.5 occurred on 15 and 16 September 2019 (marked as 1 and 2 in panel (g) of Fig. 5). Detailed investigation of these two earthquakes was not possible due to insufficient data prior to the earthquake.

Following the second earthquake, two enhancements in E_x and E_y at DNC were observed on 18 and 22 September 2019. The cluster of anomalous *Z* variations was observed during 18–24 September 2019, while the Pc4 polarization ratio *Z*/*G* showed an increase above 1.0 with a maximum value of 1.2 on 22 September 2019. There were no anomalies in E_x, E_y, *Z* and a singular anomaly in *Z*/*G* from 25–28 September 2019 when an earthquake with $M = 3.8$ at a distance of 190 km from DNC occurred on 28 September 2019 in northeast direction (marked as 3 in panel (g) of Fig. 5). Co-seismic signatures could not be determined as there was an ongoing minor geomagnetic storm of -41 nT which lasted from 28 to 30 September 2019. Clusters of anomalies in *Z* and singular *Z*/*G* were seen during 30 September 2019–04 October 2019, which could be related to the recovery phase of the storm.

As the time progressed, there were singular anomalies seen in the *Z* component in the beginning of October and clusters of anomalies in *Z*/*G* without any anomaly seen in E_x, E_y till the end of October. A $M = 4.0$ earthquake occurred at distance of 400 km from DNC on 17 October 2019 to the north (marked as 1 in pink in panel (g) of Fig. 5 and in Fig. 1); no co-seismic signals were recorded.

After a quiet period of 10 days, an anomaly in E_x component was observed along with a cluster of *Z* anomaly on 28 October 2019 which lasted for three days, overlapped with *Z*/*G* anomalies. An $M = 3.5$ earthquake occurred on 28 October 2019, 200 km northeast of DNC (4 in panel (g) of Fig. 5). Co-seismic fluctuations in *Z* and *Z*/*G* can be associated with the effects of concurrent minor geomagnetic storm with *Dst* -41 nT during 28 October-03 November 2019.

In the beginning of November, all the components remained quiet with a weak decrease in E_x and E_y on 07 November 2019 (1 mV/m) at DNC. There were singular anomalous patterns seen in *Z* component from 04 to 07 November 2019 which was seen in *Z*/*G* as a cluster on 04–07 November 2019. A $M = 4.1$ earthquake occurred at 74 km distance from DNC to the north (5 in panel (g) of Fig. 5) on 12 November 2019. No co-seismic signatures were observed in E_x and E_y but anomalous clusters in *Z* and *Z*/*G* continued till 14 November 2019. A $M = 5.0$ earthquake occurred on 19 November 2019 at 139 km from DNC due east (marked as 6 in panel (g) of Fig. 5). Co-seismic fluctuations were noted only in *Z*/*G*.

Th extent of *Z* and *Z*/*G* anomalies were observed during 22–25 November 2019 with no corresponding signatures in E_x and E_y. On 27 November 2019, there was a sharp increase/decreases in E_x/ E_y component along with further enhancement in *Z*/*G* with no anomalous Z. A $M = 4.6$ earthquake was recorded on this day, which occurred 400 km from DNC in the northeast direction (marked as 2 in pink in panel (g) of Fig. 5). Co-seismic signatures were detected in E_x, E_y, Z, *Z*/*G*.

From 01 December 2019, PTY site was also operational. It was interesting to note that there was a singular anomaly in the E_y component of PTY on 07 December 2019 with no signatures in the E_x component of PTY and E_x and E_y components of DNC. There were anomaly clusters seen at DNC from 05 to 12 December 2019 with clusters of *Z*/*G* anomaly from 05 to 08 December 2019. The *Z* at PTY showed a singular anomaly on 02 December 2019 and 12 December 2019. On 13 December 2019, there was a sudden increase/decrease in E_x/ E_y at PTY of around 10 mV/m with no counter signature at DNC, which were the co-seismic signatures of an $M=3.8$ earthquake at 165/56 from DNC/PTY in northwest direction (marked as earthquake 7 in panel (g) of Fig. 5). Post-earthquake signals in form of cluster and singular anomalies in *Z/G* were observed till 17 December 2019 at PTY. The E_x and E_y at both sites showed anomalous pattern from 14–20 December 2019 with duration 24 h of lead and lag time between the two sites. During this period, *Z* showed singular anomalies at DNC and cluster of anomaly at PTY. There was no anomalous signature in *Z/G* at DNC, but there were clusters of *Z/G* anomaly at PTY during 14–20 December 2019.

At DNC, there were cluster of *Z* anomalies during 24–27 December 2019 with no other signatures in electric or magnetic field at PTY. E_y component showed a weak anomaly on 28 December 2019 at DNC, and a cluster of *Z/G* initiated on this day which lasted for five days. At PTY, there was no anomalous signature seen in E_x and E_y during 20–31 December 2019. *Z* and *Z/G* showed cluster of anomaly beginning 28 December 2019 which lasted for 4 days. Earthquake of $M=3.6$ at 79/59 km from DNC/PTY occurred on 01 January 2020 due east (marked as 8 in panel (g) in Fig. 5). There was anomaly in E_x and E_y at DNC and PTY on the n *ext* day, with E_x anomaly at PTY on 05 January 2019. Both *Z* and *Z/G* anomalies lasted until 03 January 2020 and 07 January 2020 at DNC and PTY, respectively. During this period, there was an earthquake of magnitude $M=3.8$ at distance of 285/265 km from DNC and PTY to the west on 05 January 2020 (marked as 9 in panel (g) in Fig. 5).

The electric fields E_x and E_y at DNC and PTY were seen to fluctuate abruptly during 08–18 January 2020 along with simultaneous *Z* and *Z/G* anomaly seen during 08–18 January 2020 with singular patterns at DNC and clusters at PTY. On 12 January 2020, there were four earthquakes with magnitudes varying between $M=3.7$–4.1 at a distance of 190/177 at DNC/PTY to the east (marked as 10–13 in panel (g) in Fig. 5). Coseismic signatures in E_x, E_y at DNC and PTY and *Z* and *Z/G* only at PTY were noted.

The electric fields at both sites did not show any anomalies during 18–27 January 2020 with singular *Z* and *Z/G* anomalies seen at both DNC and PTY. On 28 January 2020, there were anomalies seen in E_x and E_y components at DNC and PTY with no *Z* anomaly at both sites and singular *Z/G* during 28–31 January 2020. An earthquake of $M=4.2$ at distance 207/180 from DNC/PTY to the east occurred on 28 January 2020 (marked as 14 in panel (g) in Fig. 5). Coseismic in *Z/G*, E_x and E_y is detected at both sites.

In the beginning of February, there were weak signatures of E_x and E_y at both DNC and PTY. There were no *Z* anomaly at DNC and singular *Z* at PTY although the sporadic *Z/G* anomaly is seen at both DNC and PTY during 03–11 February 2019. On 08 February 2020, there was an earthquake of magnitude $M=4.4$ at 136/85 km form DNC/PTY in the N/S direction (marked as 15 in panel (g) of Fig. 5). E_x shows an anomaly on 13 February 2020, and signals in *Z* and *Z/G* were observed at both sites.

4.5 Anomalous change in high frequency Pc1

We scan through the induction coil data available for a month at the DNC site. It is seen that there is only one Pc1 event observed during 1930–2330 h (duration 2 h) on 27 September 2019, shown in Fig. 6. The frequency showed a spread within 0.2–1.2 Hz in the *X* and *Z* components with a higher amplitude in X component. This spread in frequency is unusual which rather should appear as a monochromatic continuous signature during quiet geomagnetic conditions with very low *Kp* and *Dst* variation. The superposition of earthquakes around this event showed an earthquake of magnitude 3.7 to occur 10.5 h after the Pc1 event on 28 September 2019 (as indicated as earthquake 3 in Fig. 5g).

5 Discussion

Earthquake prediction falls into the following three types depending on the timescale considered: long-, medium- and short-term prediction. Long-term prediction involves a timescale of hundreds to thousands years, which can be studied on the basis of plate tectonics, activity of earthquakes, anecdotal records, fault records, archaeological survey, etc. Medium-term prediction involves a few decades to a few years, and uses databases of seismicity and crustal movements. Short-term earthquake predictions are based on reliable earthquake precursors and are a contentious issue. Published literature has documented a large variety of EM precursors for a range of large earthquakes, the locations of which span from Japan to Sumatra, Himalaya to the Andes. Examples of such studies are provided in Table A2 in Appendix. An example of a robust experiment to detect seismo-geomagnetic anomalies was conducted in Taiwan over a period of thirteen years with recording of total field at seven stations and one reference station. Significant enhancements were noted up to one month before three earthquakes including the 7.6 M Chi-Chi earthquake of 1999, which were attributed to changes in underground conductivity during earthquake preparation stage (Liu et al. 2006). Chen et al. (2010) have included information of the fault locations, fault plane solutions along with the same data to examine the relationship of earthquake epicentres and magnitudes of enhancements for 38 earthquakes of $4<M<6$ and reported observation probabilities of nearly 100% of anomalous signatures.

Over the last eight decades, many efforts have been made to examine relation between electrical phenomena in various parts of the world on the basis that compression in rocks decreases rock resistivity parallel to the compressive force (Dmowska 1977). Electrical measurements from a 6-station network in the zone of the Tangshan earthquake of 1976 detected significant resistivity decrease, which began 3 years prior to the earthquake, with maximum decrease near epicentre, and enhanced anomalies 2–0.5 months prior to the earthquake (Zhao and Qian 1994). Geoelectrical fluctuations that do not correspond to magnetic activity rise rapidly with magnitudes greater than baseline variations (1–10 mV/m) have been called Seismic Electric Signal (SES) which have been reported to start a few weeks before an earthquake occurrence and end a few days before the event (Thanassoulas et al. 2008). The VAN method was developed in Greece and uses short-separation and long-separation electrodes in conjunction with seismic data for short-term earthquake prediction. Dologlou (2008) has investigated the Brune stress drop values for 14 large earthquakes in Greece and SES lead time values and found that higher stress drop values are preceded by shorter lead times. Fidani (2012) has reported distinct power spectrum signatures of increased intensity correlatable with seismic activity. Fujinawa et al. (2011) have reported detection of electrical anomalies simultaneous with start of fault rupture in Hokkaido, Japan, and invoked the role of electrokinetic effect through increased pore pressure activated by the seismic pulse. Helman (2020) has explained that use of long time series of data as well as reference stations outside seismic zone can considerably enhance robustness of identification of anomalies related to seismic activity.

Hayakawa et al. (2000) and references therein had propounded that ULF range 0.005–10 Hz is one of the prospective bands for signatures of earthquake related phenomena. The skin depths of ULF waves depend on wave period and geo-electric structure, giving rise to two possible ULF sources: (i) those produced directly by telluric current systems originating in the stress fields of earthquake preparation zones and (ii) those ULF signals which are generated in the magnetosphere but are modified due to the effects of subsurface conductivity changes in the area near a potential earthquake. The latter would also be accompanied by variations in the geoelectric structure. Lithospheric ULF emissions are not affected by *Kp* and solar wind parameters, and this criterion has been applied to our data to remove all data correlated with *Kp* and solar wind parameters. The polarization ratio *Z/H* should increase when the conductivity beneath the site decreases. Molchanov et al. (2004) suggested that depression of amplitudes of ULF emissions can be caused by AGW generated ionospheric density and electric field disturbances. Schekotov et al. (2013) have analysed ULF variations from Karymshino Observatory in Kamchatka and outlined mechanisms of enhanced plasma concentration and changes in conductivity and/or decrease in ionospheric sources spatial scales caused by seismo-induced AGW, through which such emissions may be explained. Scoville and Freund (2015) have conducted experiments to show that using an observation network of magnetic pulses it is possible to locate epicentres of future earthquakes.

Currie and Waters (2014) have examined the power in ULF Pc3-5 (10–600 s) bands and demonstrated that the ratio of spectral powers is a promising parameter in the identification of ULF precursors by efficient distinction between space and seismogenic ULF waves. Takla et al. (2018) reported anomalous fluctuations and amplitude enhancements of Pc3 emissions from several months of data in the Sumatra region about 2 weeks prior to the occurrence of an earthquake. Ahadi et al. (2015) used *Z/H* ratios at 0.06 Hz to extract anomalous ULF signatures again in the Sumatra region. Th E_y emphasized the importance of using a suitable reference station and reported larger lead time for larger magnitude earthquakes and smaller lead time for earthquakes of increased focal depths.

In the present study, we have examined the recurring generation of anomalous signatures in E_x, E_y, Z and polarization ratios associated with occurrence of moderate magnitude earthquakes in an active section of the Kumaun Himalaya. During the approximately five months of available data, we find a consistent pattern in the time separations between the precursory signatures and the earthquakes. Table 1 includes the details of all earthquakes along with their location in comparison with the site and the anomaly patterns observed. From the trends of detected anomalies and occurrence time of earthquakes, we observe that on an average the electric field shows an anomalous signature prior to two weeks of the earthquake, followed by a quiet variation in electric field and a sudden change on the earthquake day, occurring as a co-seismic signature. The magnetic field and ULF polarization ratios are seen to start with the anomaly in electric field and show a gradual decrease in strength prior to the earthquake. This has been explained as the small attenuation associated with lower frequencies of ULF waves which allows the propagation of these waves in lithosphere over long distances (Nagao et al. 2002). In the discussion below, we have taken the interval between the most prominent signature (either in E_x/ E_y or Z) and the following earthquake, as the lead time for that seismic event. The polarization ratios being much more abundant may not provide unambiguous lead times but is indicative of a generally active nature of the area of study. As shown in our study, active seismic zones intermittently record earthquakes of varying magnitudes; thus, the recording of anomalous signatures in *Z/G*, Z, E_x/ E_y is continual, when observed from appropriate distances from the epicentres.

During the period of observation, six earthquakes of $3.5 > M > 4.0$ occurred, four of them to the east and two to the northwest. Of the four eastern epicentres, three were 190/170 km from DNC/PTY while the fourth was at 70/60 km from DNC/PTY. Anomalous signatures of E_x/ E_y, Z, *Z/G* were observed with comparable amplitudes and lead times varying between 3 and 10 days; the lead time decreases with increase in magnitude of EQ. The northwestern epicentres are 165/56 km and 285/265 km from DNC/PTY. Anomalies

Table 1 Details of earthquake, anomaly patters in E_x, E_y and z anomaly

Sl. no. (Eq magnitude)	Distance from site DNC/PTY (km)	Azimuthal relation to DNC/PTY	Absolute amplitude of anomaly DNC, PTY (days prior to earthquake at each site) δ stands for deviations of ± 1 mV/m for E_x and E_y and ± 5 nT along with consideration of IQ and ID days (not applicable indicates data not available) and (no indicates signal is absent)			Z/H anomaly (observed prior to earthquake in days)
			δE_x (mV/m)	δE_y (mV/m)	δZ (nT)	
Equation 1 (4.0)	225/210	NE/E	Not applicable	Not applicable	Not applicable	Not applicable
Equation 2 (4.5)	130/100	NE/SE	Not applicable	Not applicable	Not applicable	Not applicable
Equation 3 (3.8)	190/155	NE/SE	0.5 (10 days), NA	1.2 (10 days)	7 (7 days)	7
Equation 4 (3.5)	200/185	NE/SE	No	NO	5 nT (11 days)	11
Equation 5 (4.1)	74/22	NE/SE	1.2 (5 days), NA	1.3 (5 days)	1 nT (1 day)	3
Equation 6 (5.0)	139/144	E/SE	1.2 (5 days), NA	1.1 (5 days)	2 nT (1 day)	1
Equation 7 (3.8)	165/56	NW/NW	1.3 (15 days), 1.2 (8 days)	1.8 (15 days) 2 (8 days)	7.404 nT, 4.104 nT (12 days)	10
Equation 8 (3.6)	79/59	NE/SE	No, 28 (13 days)	No, 8 (13 days)	1.45 nT, 0.65 nT (4 days)	4
Equation 9 (3.8)	285/265	NW/NW	34 (3 days)	8 (3 days)	2 nT, 3 nT (3 days)	3
Equations 10–13 (4.1)	190/177	NE/SE	3.618 (4 days), 19 (4 days)	4 (4 days)	0.2, 2 (4 days)	5
Equation 14 (4.2)	207/180	NE/SE	4, 1.2 (13 days)	1.5, 2 (13 days)	5, 1 (1 day)	5
Equation 15 (4.4)	136/85	N/S	3 (10 days) 8 (10 days)	2.885 (6 days) 2.8 (6 days)	1 nT, 2nT (7 days)	7

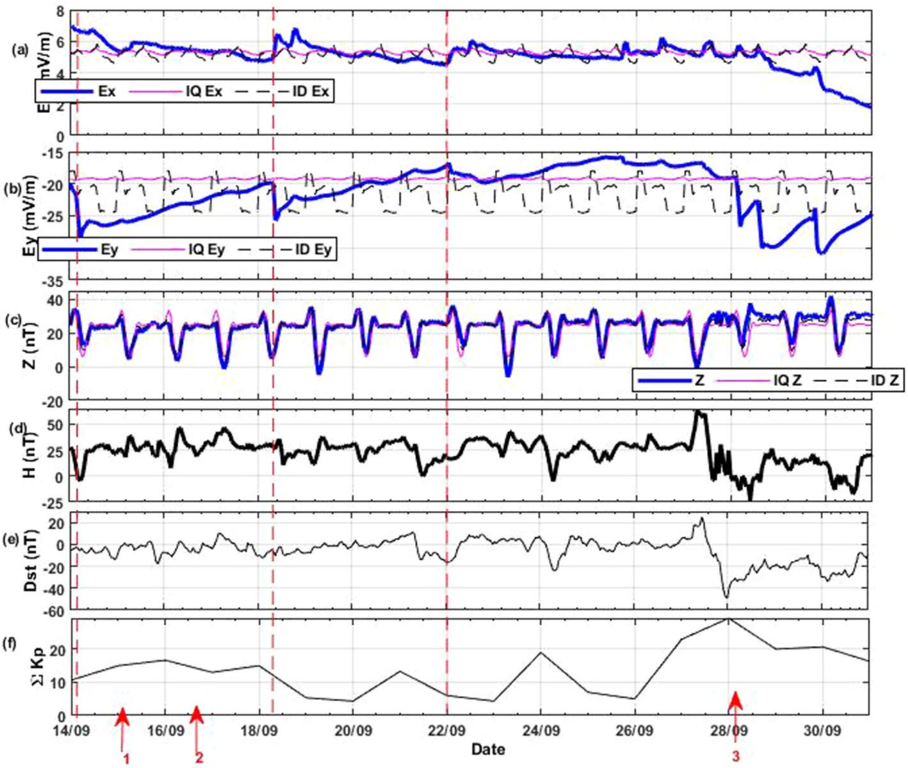

Fig. 2 Hourly variation in electric field E_x (panel **a**) and E_y (panel **b**) during 14–30 September 2019 at DNC. Average variation in electric field of IQ and ID days is superimposed. The dashed lines mark the anomalous electric and magnetic fields

in all components are observed, with those at DNC showing higher amplitudes. For the EQ of epicentre 165/56 km, lead time is 15/8; for the other lead time is 3/3 at DNC/PTY.

Of the five earthquakes of $4.0 > M > 4.5$, three occur in N-S trend between PTY and DNC; the other two have epicentres due east; epicentral distances vary 75–400 km from DNC; amplitudes of Z anomalies increase with decreasing epicentral distance. The EQ occurring between DNC and PTY has negligible to weak electric field anomalies and strong anomalies in Z and Z/G, with lead times of between 3 and 5 days. The two eastern epicentres are at 460 and 190/175 km from DNC/PTY. Anomalies of comparable amplitudes are observed in all components with increased amplitudes for larger magnitude EQ, with lead times of 4 days.

One EQ of $M = 5.0$ occurred 139 km from DNC to the northeast. Anomalies are observed in all the components and lead time is 5 days. Thus, we summarize that the earthquakes which occurred to the east and northeast of DNC/PTY produced prominent anomalies in E_x/ E_y, whereas those between the two sites have weak electric field signatures. We ascribe this azimuthal preference to the geometry of subsurface conductivity. Amplitudes of anomalies in Z are a function of both magnitude of earthquake and epicentral distance; the former appears to have a stronger influence. Observations of more earthquakes from a larger number of sites of varying distances and azimuths are required to resolve this

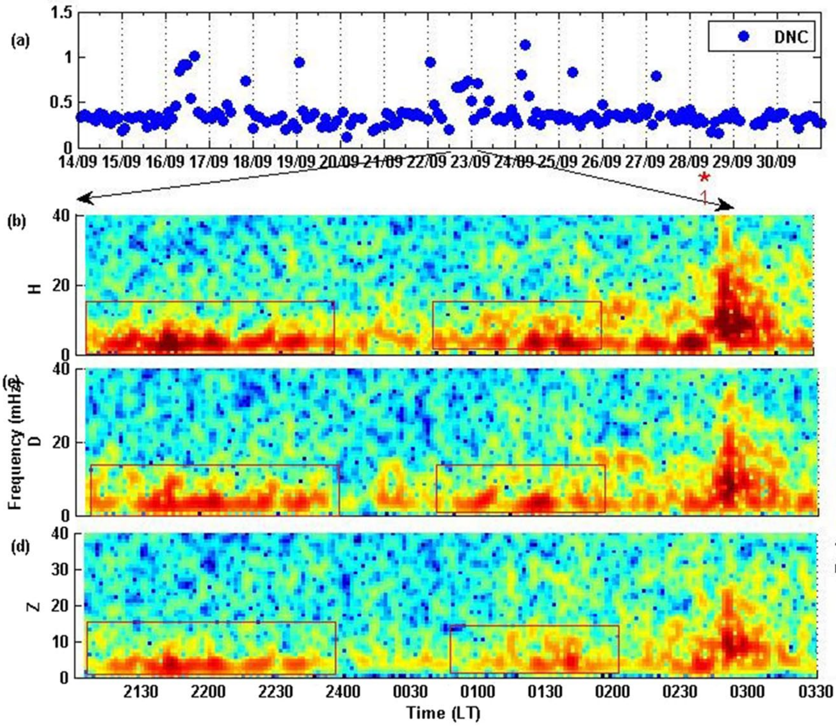

Fig. 3 **a** Estimation of polarization ratio from night-time Pc4 pulsation in frequency band of 10 ± 3 mHz during 14–30 September 2019. The spectral estimates of amplitude and frequency for 22 September 2019 are showed for *H* (**b**), *D* (**c**) and *Z* (**d**) components for DNC, respectively

relationship better. Lead times appear to have an inverse relationship with the magnitude of the earthquake, i.e. the larger the magnitude the smaller the lead time. However, based on the observations of EQ 7, we see that the site which is significantly farther records precursor anomalies with longer lead times. For other earthquakes recorded at both the sites, the differences in epicentral distances were not sufficient to make resolvable differences in lead time. Prima facie it appears that lead times may be linked to the actual area, which is undergoing stress variations prior to the impending earthquake: if the observation site is nearer to the outer edge of this area, lead time of observation will be longer.

Some anomalies in the form of singular *Z* and the cluster of *Z*/*G* were observed during 04–10 October 2019 at DNC and during 13–21 February 2020 at DNC and PTY without any association with electric field anomalies or earthquake occurrence. Both occurred during the recovery phases of moderate magnetic storms; we infer that in such cases false positive anomalies may be produced (Fig. 5).

To summarize, in our study we have observed enhancements in the *Z* component 1–2 weeks prior to all the earthquakes considered, without corresponding changes in the *H* component. No co-seismic enhancements are noted, however. The data indicate steady changes in electrical measurements 3–10 days prior to each earthquake. For the eight earthquakes, we see increase in E_x and decrease in E_y, whereas for 2 earthquakes we see decrease in E_x and increase in E_y. Whether this may be indicative of change in direction

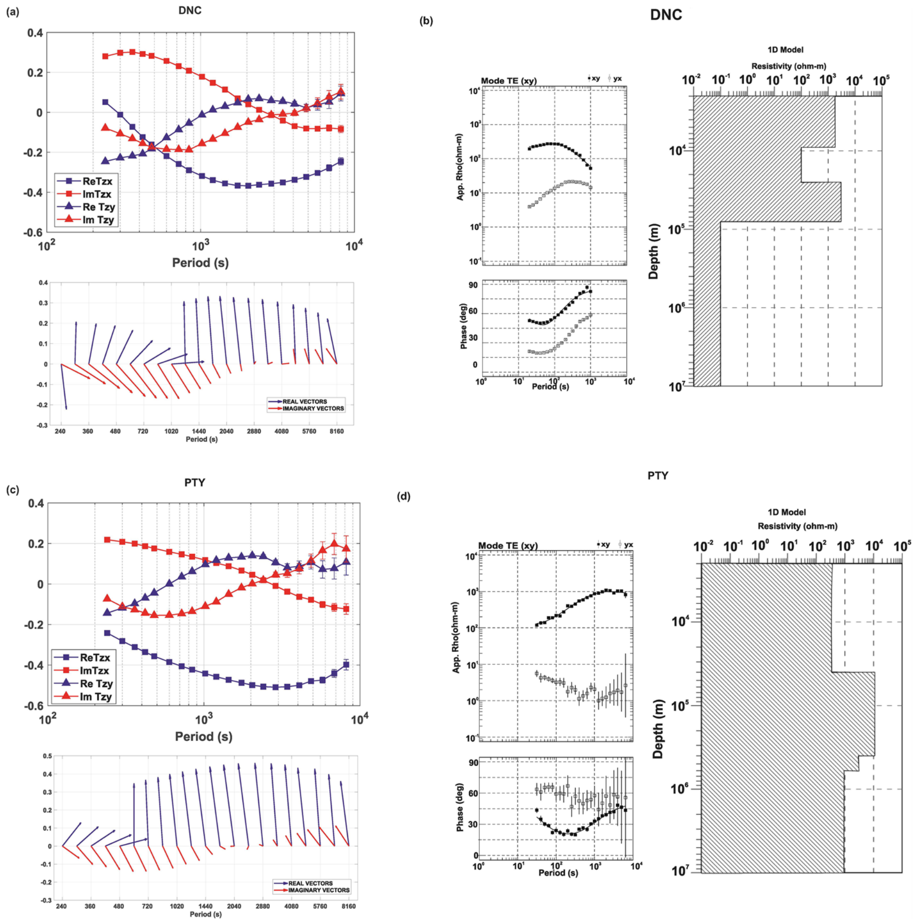

Fig. 4 GDS and LMT results at DNC **a** observed tippers (top panel) and the Parkinson convention induction arrows (bottom panel), **b** observed and computed responses of apparent resistivity and phase curves (left panel) for 1D inversion model (right panel). GDS and LMT results at PTY, **c** observed tippers (top panel) and the Parkinson convention induction arrows (bottom panel), **d** observed and computed responses of apparent resistivity and phase curves (left panel) for 1D inversion model (right panel)

of principal compressive force for different earthquakes can be established with observations over a longer period (Fig. 7). For 2 more earthquakes, we see anomalous pattern only in E_x component. The variation does not have a strong causal model. The anomalous E_x/ E_y changes occur prior to the Z enhancements by 2–3 days to few hours. This could be due to the changes in the conductivity due to stress build-up. For earthquakes of magnitude 3.6–3.9, the E_x/ E_y anomalies are seen 10 days and magnetic Z field anomaly is seen 4–11 days prior to the earthquake except for EQ7 (occurred NW of the site) for which the anomalies are seen prior to 3 days. For earthquakes with magnitude 4.0 and above, the anomaly in E_x/ E_y is seen 4–7 days prior to the earthquake along with coseismic signatures at one of the sites and Z enhancements are seen prior to 2 days to few hours (Fig. 7). In addition, it is seen that for the period for which both the stations were operational, the pattern of inter-relationships are same at both the sites for EQ 7 and EQs 9–11. For earthquake

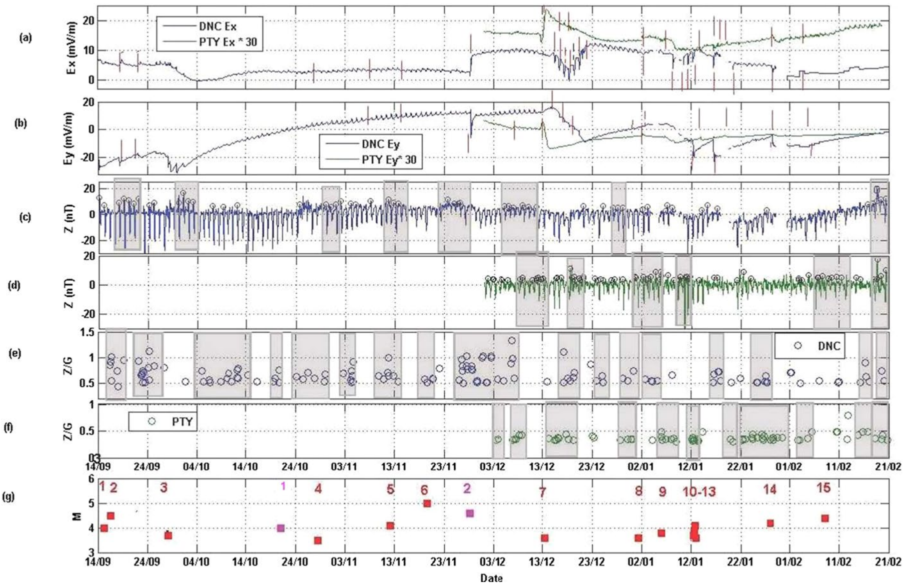

Fig. 5 Variation in raw parameters recorded at DNC and PTY: electric field (**a**) E_x, (**b**) E_y, magnetic field (**c**) Z, (**d**) H, polarization ratio at (**e**) DNC, (**f**) PTY. Earthquakes that occurred during the period of investigation are included in (**g**)

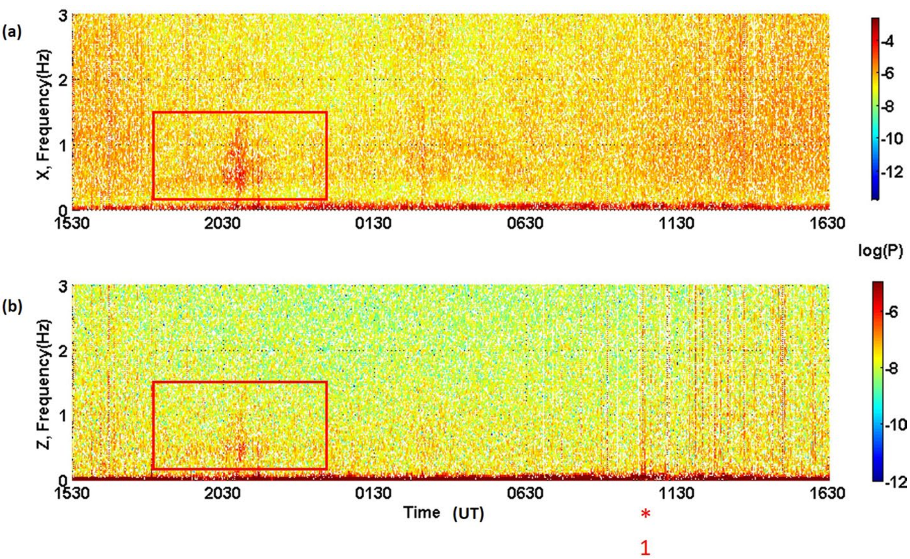

Fig. 6 Evolution of Pc1 event during 1930–2130 h on 27 September 2019 at DNC in the *X* (top) and *Z* (bottom) panels, respectively

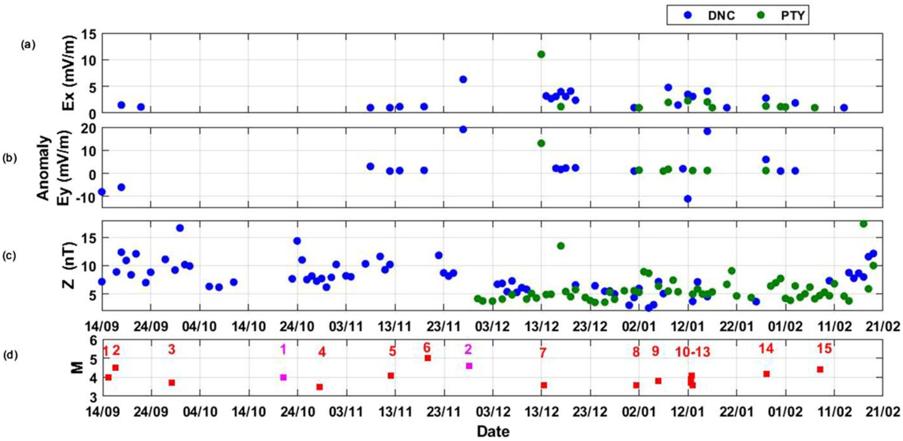

Fig. 7 Variation in anomalous electric and magnetic field at DNC and PTY **a** E_x, **b** E_y, **c** Z. Panel (**d**) represents the earthquakes. Right upper and lower panel shows the schematic variations in electric field and magnetic field in relation to earthquake, respectively

8, the anomalies are seen only at PTY. Shorter lead times for the larger earthquakes could be explained by the rapidness of stress drop.

The signatures of night-time Pc4 anomaly mimic the *Z* anomalies. The ULF anomalies in Pc4 amplitudes show enhancements for all earthquakes, and this could be due to conductivity/plasma concentration changes which reinforced the strength of the reflected wave of Pc4 as suggested by Yumoto et al. (2009). We observe the trend of occurrence patterns of the Pc4 as a week to few weeks. The amplitudes of these emissions show a trend of decrease/increase from the time of initial occurrence to 1–3 days prior to the occurrence, viz. this pattern is most prominent in the case of 8 earthquake(s) of 3.5–5.0 magnitude, which occurred in the NE/E of the recording site. This may be inferred to be due to the role of AGW, which has perturbed the ionosphere. In order to better infer the temporal relation of the anomalies of magnetic fluctuations with earthquakes, we perform a super posed epoch analysis using the median values of *Z* and polarization anomaly which lied above their respective median values and the results are shown in Fig. 8. The scale of the polarization anomaly is increased by twice to fit into the ordinate scale. The median values of *Z* and *Z*/*G* are plotted around ± 8 days of the onset of the earthquake.

A clear increase in *Z* is observed during local night for a week to 4 days prior to the earthquake which reduced on the earthquake day and then shows an increase. Similarly, *Z*/*G* also shows an increase before 4–6 days of earthquake, then shows a decrease and peaks on the earthquake day. This *Z*/*G* remains steady for 2 days after the earthquake before showing a decrease. We have earlier noted that *Z*/*G* anomalies are profuse in number, which increases uncertainties when they are designated as precursors. On the other hand, examination of data from an aseismic site (HYB) shows the complete absence of anomalous pulsations during the same time interval (Figure A3 in Appendix). This further suggests that the observed pulsations in the seismic site are of lithospheric origin.

It should be noted that although a temporal variation is obtained, but there exists a clear chance of ambiguity on association of an observed anomaly with the earthquake that they precede. This is because there are other degrees of freedom related to the preparation of earthquake which include the fault system, direction of strike, type of fault system which

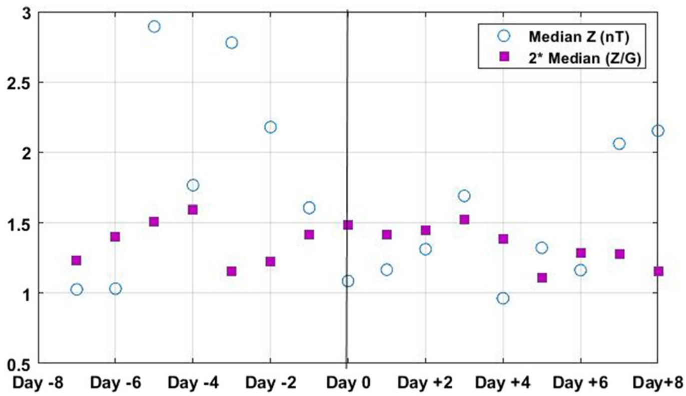

Fig. 8 Variation in median values of night time values of anomaly in *Z* and *Z/G* around the onset of earthquake for ± 8 days

can control the flow of energy. A better control on these independent parameters can be achieved by considering a bigger grid with more number stations placed as a grid around the fault system. Examples of studies based on extended networks of multiple sensors from China and the USA are provided in the works of Huang et al. (2017) and Heavlin et al. (2022). Huang et al. (2017) provided a 50-year review of earthquake prediction science and sustainability in China in the background of the successful prediction of the February 4th, 1975, 120 Haicheng Ms7.3 earthquake based on data from a network of seismometers, which was followed by the missed prediction of the 1976 Tangshan Ms7.8 and the 2008 Ms8.0 Wenchuan earthquakes and remain as classic examples of failures. Further, they discussed the approach of hierarchical analyses of multiple earthquake precursors and production of country-wide forecast maps based on statistical analyses. Heavlin et al. (2022) present an analysis of ground-based magnetic time-series measurements before 19 earthquakes ≥ M4.5 in California drawing from over 330,000 site-days of measurement spanning a decade. They conclude that 'there is a physical change that can be observed in the days before an earthquake, but further scientific study is needed to understand this process'.

The potential for short-term predictions is based on the earthquake science of dynamic failures of faults and associated the micro-fracturing and/or quasi-static preslip. Earthquake precursors are generated by these processes; hence, a physics-based approach to diagnose them appears to be feasible even in the light of the complexities involved. Recently, there is growing understanding that small and large earthquakes are indistinguishable until the rupture process comes to a halt. This implies that the lithospheric processes prior to an earthquake, which generate the precursors, would not necessarily represent the true nature of the impending event. Thus, approaches to reliable precursors of earthquakes and the possibility of predicting their occurrence continue to be a matter of intense debate within the scientific community, with strong arguments both in favour of and against.

In the past decades, the work of Fraser-Smith et al. (1990) on the identification of ULF precursors of the Loma Prieta earthquake was refuted by Campbell (2009), whose analysis showed that the ULF signal was not local but rather widespread throughout the western United States and due to a coincidental geomagnetic solar-terrestrial disturbance field. In response, Fraser-Smith et al. (2011) published a re-analyses and re-affirmed the existence of large amplitude fields, which could be explained as generated by lithospheric perturbations. Masci and Persio (2012) challenged the findings of ULF anomalies prior to the L'Aquila 2009 seismic sequence, presented by Eftaxias et al. (2009, 2010) and demonstrated the complete absence of any associated magnetic anomalies. Masci and Thomas (2013a) further challenged the work of Ida et al. (2012) showing that decreases in fractal dimensions of ULF anomalies associated with the China earthquake of 1 September 2003 were in fact due to regular patterns of geomagnetic fluctuations. Masci and Thomas (2013b) also reexamined the work of Hayakawa et al. (2004) on the ULF anomalies associated with the 2000 Izu swarm and claimed that the behaviour of the Hurst exponent was strongly related to the level of global geomagnetic activity and not to the increase in the local seismic activity. Masci and Thomas (2015a, b) have questioned the concept of use of polarization ratio variations as indicators of impending earthquakes and have also challenged the use of Spatial Scintillation Index as ionospheric precursors. Pham et al. (2002) analysed observed transient electric signals in Greece, very similar to the seismic electric signals by the VAN method and ascribed them to two electrochemical mechanisms and cautioned against associating them to earthquake phenomena. The counter-arguments against the effectiveness of VAN methods can be listed as follows: (1) SES are noise, (2) the success and alarm rates are not as high as the VAN group claims, (3) such a success rate can be achieved by chance and (4) the VAN method can provide many false positives (Helman 2020). Pham and Geller (2002) have demonstrated the similarities between VLF signals due to lightning and those ascribed to seismic activity by Eftaxias et al. (2001), thereby raising doubts on their significance. In a recent work, Wang et al. (2022) have classified ULF signals into atmospheric, tectonic, cultural and instrumental and demonstrated on the basis of a large volume of data from Quakefinder mission that signals before the 2007 October 31 Alum Rock M5.4 earthquake near San Jose, California, were not in fact seismic in nature.

In our study, we have examined a combination of anomalies in electric and magnetic fields and find apparent association with earthquake occurrence. Thus, we argue that the observed electromagnetic anomalies are of seismogenic origin, and although the mechanism is elusive, rigorous observation can lead to earthquake prediction in future.

The basis of correlation of EM (and indeed any other) signals with that of earthquake occurrences intrinsically depends on the use of earthquake catalogues, which provide origin time, location and magnitude of earthquakes regionally or globally, over the time span of instrumental measurements of seismic waves. Different agencies may adopt different techniques to produce earthquake catalogues, leading to heterogeneity of catalogues over the same time span and covering the same region. Further the density and coverage of the network of seismometers impact the extent of systematic and random errors which creeps into the calculation of the earthquake parameters, particularly true for the smaller magnitude earthquakes, e.g. magnitude comparison of events common to different catalogues in Italy shows underestimation by one catalogue (Storchak et al. 2000). In our study, we have used that ISC catalogue as a reliable source sustainable over long time spans; however, the actual magnitudes and locations are expected to suffer from inaccuracies. This is an inherited problem of investigating EM signatures of moderate magnitude earthquake sequences, which implicitly constrains quality of statistical predictions.

While Wyss and Allman (1996) emphasized the lack of plausible explanations behind observed anomalous signals in electrical–magnetic data as well as lack of statistically significant correlations with individual earthquakes; nevertheless, Wyss (1997) pointed out the flaws in the reasoning of Geller (1997) and emphasized that with enough understanding of earthquake mechanics and improvements in detection levels, earthquake prediction may be a possibility for the future and efforts to do so need to be pursued seriously. Main (1999) also debated along the same lines. Wyss (2001) has expressed that 'as a physical phenomenon, earthquakes must be predictable to a certain degree'. Uyeda and Nagao (2018) and Hayakawa (2018) have expressed their faith in the future of research in earthquake prediction. An exhaustive review of precursors from ground data, provided by Conti et al. (2021), discusses seismo-electromagnetic precursors have been discussed in detail, beside mechanical, geochemical, thermal precursors. Approaches for recognizing natural and artificial electromagnetic background have been discussed in an effort to enhance the robust identification of signals of seismic origin. The understanding of earthquake physics is essential to the understanding of precursor diagnostics. Nakatani (2020), Picozza et al. (2021) have also supported this approach. Szakacs (2021) has also argued in favour of a long-term approach to earthquake precursor analysis.

Optimized EM monitoring of regions around active faults will yield information about the prevalent mechanisms which are at play. Such mechanisms would change with time, hence long time monitoring is a must. Our observations of the data show that apart from geomagnetic, ionospheric and seasonal characteristics, local geological conditions of the data recording sites need to be considered for realistic definition of anomalous signatures. Hence, in the ongoing stage of establishing the science of earthquake precursors, we feel that design of observation experiments has to be conducted specific to the targeted seismogenic faults to produce meaningful results. Our pilot study adds further confirmation to the already existing volume of literature that stress build-up processes, which are a pre-requisite for an earthquake event, generate electromagnetic signals of different kinds and frequencies. Even apart from having potential as precursors, the study of EM signals, in combination with other geophysical parameters, can provide substantial inputs to the understanding of physics of earthquake processes.

6 Conclusion

From the present study, we conclude that

(i) medium- to long-term observations of electric and magnetic fields in and around a seismogenic are necessary to define robust anomalous signatures, which would be specific to that area
(ii) a combination of electric and magnetic field observations are necessary to reduce ambiguity, installation of a network along with radon measurements could greatly enhance the strength of the statistical analysis
(iii) an appropriate geometry of observation sites with recordings of electric and magnetic fields would allow the combination of anomalies to be identified, based on which the relations among magnitude and epicentral distance of earthquakes vis-à-vis trends, amplitudes and lead times of precursory EM signatures can be deciphered
(iv) initial patterns of EM precursors in the Kumaun Himalaya are promising and justify follow-up.

More observation and data acquisition are underway that could lead to successful prediction. For a successful prediction tool, it is essential to obtain electric and magnetic data that are azimuthally located wherein a gradient analysis also can be used.

Supplementary Information The online version contains supplementary material available at https://doi.org/10.1007/s11069-023-05844-y.

Acknowledgements The authors acknowledge all the public domain data sets for the availability geomagnetic data activity indices from CDAWEB (https://cdaweb.gsfc.nasa.gov/ind E_x.html/) and earthquake data from obtained from the ISC catalogue (http://www.isc.ac.uk/). Authors thank Director, CSIR-NGRI and Project leader of SHIVA for the support to make this experiment. Jayashree Bulusu thanks *DST*-INSPIRE for her Fellowship. Authors acknowledge the team of observatory staff especially Srinu Yadavally and N. Phani Chandrasekhar for their contribution in carrying out the strenuous field work in Himalayan region. This is an original NGRI contribution NGRI/Lib/2020/Pub-35. Dr. Tarun C. Khanna is thanked for his guidance on the geological setup of the two recording sites. The authors thank the anonymous reviewers for their thorough and constructive evaluation of the work and the Editor-in-Chief John Clague for his patient support throughout the review process.

Author contributions All authors contributed to the study conception and design. Material preparation, data collection and analysis were performed by JB, SS and AE. The first draft of the manuscript was written by JB and KA, and all authors commented on previous versions of the manuscript. All authors read and approved the final manuscript.

Funding This work was supported by Director, CSIR-NGRI and SHIVA Project (grant number: MLP-FBR-0003).

Data availability All the data are available with authors and will be made available in public domain via NGRI Data Center.

Declarations

Conflict of interest The authors declare they have no conflict of interests with regards to this work.

References

Ahadi S, Puspito N, Ibrahim G, Saroso S, Yumoto K, Yoshikawa A, Muzli L (2015) Anomalous ULF emissions and their possible association with the strong earthquakes in Sumatra, Indonesia, during 2007–2012. J Math Fundam Sci 47:84–103. https://doi.org/10.5614/j.math.fund.sci.2015.47.1.7

Alam A, Wang N, Zhao G, Barkat A (2020) Implication of radon monitoring for earthquake surveillance using statistical techniques: a case study of Wenchuan earthquake. Geofluids 2020:1–14. https://doi.org/10.1155/2020/2429165

Astafyeva E (2019) Ionospheric detection of natural hazards. Rev Geophys 57:1265–1288. https://doi.org/10.1029/2019RG000668

Bakhmutov VG, Groza AA (2008) The dilatancy-diffusion model: new prospects. In: Proceedings of the 7th international conference "Problems of Geocosmos" (St. Petersburg, Russia, 26-30 May 2008)

Bella F, Biagi PF, Caputo M, Cozzi E, Monica GD, Ermini A et al (1995) Helium content in thermal waters in the Caucasus from 1985 to 1991 and correlations with the seismic activity. Tectonophysics 246(4):263–278. https://doi.org/10.1016/0040-1951(94)00260-G

Bortnik J, Cutler J, Dunson C, Bleier TE (2008) The possible statistical relation of Pc1 pulsations to Earthquake occurrence at low latitudes. Ann Geophys. https://doi.org/10.5194/angeo-26-2825-2008

Bulusu J, Prasanna Simha C, Arora K, Rao KM (2020) Statistical characteristics of low latitude Pc4s: Influence of Solar wind and IMF parameters. Adv Space Res. https://doi.org/10.1016/j.asr.2020.01.001

Campbell WH (2009) Natural magnetic disturbance fields, not precursors, preceding the Loma Prieta earthquake. J Geophys Res 114:A05307. https://doi.org/10.1029/2008ja013932

Carbone V, Piersanti M, Materassi M, Battiston R, Lepreti F, Ubertini P (2021) A mathematical model of lithosphere–atmosphere coupling for seismic events. Sci Rep 11:8682. https://doi.org/10.1038/s41598-021-88125-7

Chadha RK, Singh C, Shekar M (2006) Transient changes in well-water level in bore wells in Western India due to the 2004 Mw 9.3 Sumatra Earthquake. Bull Seismol Soc Am 98(5):2553–2558. https://doi.org/10.1785/0120080952

Chamyal LS, Vashi NM, Shah OK (1989) Metavolcanics of lesser kumaun Himalaya. In: Saklani PS (ed) Current trends in geology, vol 12, Today and Tomorrows Printers and Publisher, New Delhi, pp 195–210

Chen CH, Liu JY, Lin PY, Yen HY, Hattori K, Liang WT, Chen YI, Yeh YH, Zeng X (2010) Pre-seismic geomagnetic anomaly and earthquake location. Tectonophysics 489:240–247. https://doi.org/10.1016/j.tecto.2010.04.018

Cieślik J (2018) Dilatancy as a measure of fracturing development in the process of rock damage. Open Geosci 10:484–490. https://doi.org/10.1515/geo-2018-0038

Cochran ES, Vidale JE, Tanaka S (2004) Earth tides can trigger shallow thrust fault earthquakes. Science 306 (5699), 1164–1166. https://doi.org/10.1126/science.1103961

Conti L, Picozza P, Sotgiu A (2021) A critical review of ground based observations of earthquake precursors. Front Earth Sci 9:676766. https://doi.org/10.3389/feart.2021.676766

Contoyiannis YF, Kapiris PG, Eftaxias KA (2005) Monitoring of a preseismic phase from its electromagnetic precursors. Phys Rev E. https://doi.org/10.1103/PhysRevE.71.066123

Crampin S, Evans R, Balamir U, Doyle M, Davis JP, Yegorkina GV, Miller A (1980) Observations of dilatancy-induced polarization anomalies and earthquake prediction. Nature 286:874–877

Currie JL, Waters CL (2014) On the use of geomagnetic indices and ULF waves for earthquake precursor signatures. J Geophys Res Space Phys 119:992–1003. https://doi.org/10.1002/2013JA019530

Dasgupta S, Pande P, Ganguly D, Iqbal Z, Sanyal K, Venkataraman NV, Dasgupta S, Sural B, Hanrendranath L, Mazumdar K, Sanyal S, Roy A, Das LK, Mishra PS, Gupta H (2000) Seismotectonic atlas of India and its environs, In: Narula PL, Acharyya SK, Banerjee J (eds) Special Publication Series 59, Geological Survey of India. ISBN: ISSN: 02540436

Dea JY, Hansen PR, Boerner WM (1993) Long-term ELF background noise measurements, the existence of window regions, and applications to earthquake precursor emission studies. Phys Earth Planet Inter 77(1–2):109–125. https://doi.org/10.1016/0031-9201(93)90037-A

De Santis A, Balasis G, Pavón-Carrasco FJ, Cianchini G, Mandea M (2017) Potential earthquake precursory pattern from space: the 2015 Nepal event as seen by magnetic Swarm satellites. Earth Planet Sci Lett 461:119–126. https://doi.org/10.1016/j.epsl.2016.12.037

De Santis A, Cianchini G, Marchetti D, Piscini A, Sabbagh D, Perrone L et al (2020) A multiparametric approach to study the preparation phase of the 2019 M7.1 Ridgecrest (California, United States) Earthquake. Front Earth Sci 8:478. https://doi.org/10.3389/feart.2020.540398

Dmowska R (1977) Electromechanical phenomena associated with earthquakes. Geophys Surv 3:157–174. https://doi.org/10.1007/BF01449191

Dologloue E (2008) Possible relationship between Seismic Electric Signals (SES) lead time and earthquake stress drop. Proc Jpn Acad Ser B 84:117–122

Dosso HW, Chen J (2000) Analogue model study of EM induction in elongated conductors—2D and 3D induction arrow responses. Earth Planet Space 52:355–360. https://doi.org/10.1186/BF03351647

Eftaxias K, Kapiris P, Polygiannakis J, Bogris N, Kopanas J, Antonopoulos G, Peratzakis A, Hadjicontis V (2001) Signature of pending earthquake from electromagnetic anomalies. Geophys Res Lett 28:3321–3324

Eftaxias K, Kapiris P, Dologlou E, Kopanas J, Bogris N, Antonopoulos G, Peratzakis A, Hadjicontis V (2002) EM anomalies before the Kozani earthquake: a study of their behavior through laboratory experiments. Geophys Res Lett. https://doi.org/10.1029/2001GL013786

Eftaxias K, Athanasopoulou L, Balasis G, Kalimeri M, Nikolopoulos S, Contoyiannis Y, Kopanas J, Antonopoulos G, Nomicos C (2009) Unfolding the procedure of characterizing recorded ultra-low frequency, kHZ and MHz electromagnetic anomalies prior to the L'Aquila earthquake as pre-seismic ones—part 1. Nat Hazard 9:1953–1971. https://doi.org/10.5194/nhess-9-1953-2009

Eftaxias K, Athanasopoulou L, Balasis G, Kalimeri M, Nikolopoulos S, Contoyiannis Y, Kopanas J, Antonopoulos G, Nomicos C (2010) Unfolding the procedure of characterizing recorded ultra-low frequency, kHZ and MHz electromagnetic anomalies prior to the L'Aquila earthquake as pre-seismic ones—part 2. Nat Hazard 10:275–294. https://doi.org/10.5194/nhess-10-275-2010

Fidani C (2012) The Central Italy Electromagnetic Network and the 2009 L'Aquila Earthquake: observed electric activity. Geosciences 1:3–25. https://doi.org/10.3390/geosciences1010003

Fraser-Smith AC, Bernardi A, McGill PR, Ladd ME, Helliwell RA, Villard OG Jr (1990) Low-frequency magnetic field measurements near the epicenter of the M,7.1 Loma Prieta Earthquake. Geophys Res Lett 17:1465–1468

Fraser-Smith AC, McGill PR, Bernardi A (2011) Comment on "Natural magnetic disturbance fields, not precursors, preceding the Loma Prieta earthquake" by Wallace H. Campbell. J Geophys Res 116:A08228. https://doi.org/10.1029/2010JA016379

Freund F (2010) Toward a unified solid state theory for pre-earthquake signals. Acta Geophys 58:719–766. https://doi.org/10.2478/s11600-009-0066-x
Fujinawa Y, Takahashi K, Noda Y, Iitaka H, Yazaki S (2011) Remote detection of the electric field change induced at the seismic wave front from the start of fault rupturing. Int J Geophys. https://doi.org/10.1155/2011/752193
Gao Y, Wang Q, Zhao B, et al. (2014) A rupture blank zone in middle south part of Longmenshan Faults: Effect after Lushan Ms7.0 earthquake of 20 April 2013 in Sichuan, China. Sci China: Earth Sci 57:2036–2044. https://doi.org/10.1007/s11430-014-4827-2
Geller RJ (1997) Earthquake prediction: a critical review. Geophys J Int 131:425
Gokhberg MB, Morgounov VA, Yoshino T, Tomizawa I (1982) Experimental measurement of electromagnetic emissions possibly related to earthquakes in Japan. J Geophys Res 87(B9):7824–7828. https://doi.org/10.1029/JB087iB09p07824
Geller RJ, Jackson DD, Kagan YY, Mulargia F (1996) Earthquakes cannot be predicted. Science 275(5306):1616. https://doi.org/10.1126/science.275.5306.1616
Han P, Qing-Hua H, Ji-Gang X (2009) Principal component analysis of geomagnetic diurnal variation associated with earthquakes: case study of the M6.1 Iwate-ken Nairiku Hokubu earthquake. Chin J Geophys Chin Ed 52:1556–1563. https://doi.org/10.3969/j.issn.0001-5733.2009.06.017
Han P, Hattori K, Hirokawa M, Zhuang J, Chen C-H, Febriani F, Yamaguchi H, Yoshino C, Liu J-Y, Yoshida S (2014) Statistical analysis of ULF seismomagnetic phenomena at Kakioka, Japan, during 2001–2010. J Geophys Res Space Phys 119:4998–5011. https://doi.org/10.1002/2014JA019789
Hattori K, Serita A, Yoshino C, Hayakawa M, Isezaki N (2006) Singular spectral analysis and principal component analysis for signal discrimination of ULF geomagnetic data associated with 2000 Izu Island Earthquake Swarm. Phys Chem Earth 31(4–9):281–291
Hayakawa M, Fujinawa Y (eds) (1994) Electromagnetic phenomena related to earthquake. Prediction. Terra Scientific Publishing, Tokyo, Japan
Hayakawa M (eds) (1999) Atomospheric and ionospheric electromagnetic phenomena associated with earthquake. Terra Scientific Publishing, Tokyo, Japan
Hayakawa M (2018) Pre-earthquake processes: a multidisciplinary approach to earthquake prediction studies, 1st edn. In: Ouzounov D, Pulinets S, Hattori K, Taylor P (eds) Geophysical monograph, vol 234. American Geophysical Union. John Wiley & Sons, Inc
Hayakawa M, Hattori K, Nickolaenko AP, Rabinowicz LM (2004) Relation between the energy of earthquake swarm and the Hurst exponent of random variations of the geomagnetic field. Phys Chem Earth 29:379–387. https://doi.org/10.1016/j.pce.2003.07.00
Hayakawa M, Kopytenko Y, Smirnova N, Troyan V, Peterson T (2000) Monitoring ULF magnetic disturbances and schemes for recognising earthquake precursors. Phys Chem Earth (a) 25(3):263–269
Hayakawa M, Schekotov A, Potirakis S, Eftaxias K (2015) Criticality features in ULF magnetic fields prior to the 2011 Tohoku earthquake. Proc Jpn Acad Ser B 91:25–30. https://doi.org/10.2183/pjab.91.25
Heavlin WD, Kappler K, Yang L, Fan M, Hickey J, Lemon J et al (2022) Case-control study on a decade of ground-based magnetometers in California reveals modest signal 24–72 hr prior to earthquakes. J Geophys Res Solid Earth 127:e2022JB024109. https://doi.org/10.1029/2022JB024109
Helman DS (2020) Seismic electric signals (SES) and earthquakes: a review of an updated VAN method and competing hypotheses for SES generation and earthquake triggering. Phys Earth Planet Inter 302:106484. https://doi.org/10.1016/j.pepi.2020.106484
Hough S (2010) Predicting the unpredictable. The tumultuous science of earthquake prediction. Princeton University Press, Princeton, p 280
Huang F, Li M, Ma Y, Han Y, Tian L, Yan W, Li X (2017) Studies on earthquake precursors in China: a review for recent 50 years. Geodesy Geodyn. https://doi.org/10.1016/j.geog.2016.12.002
Ida Y, Yang D, Li Q, Sun H, Hayakawa M (2008) Detection of ULF electromagnetic emissions as a precursor to an earthquake in China with an improved polarization analysis. Nat Hazards Earth Syst Sci 8:775–777. https://doi.org/10.5194/nhess-8-775-2008
Ida Y, Yang D, Li Q, Sun H, Hayakawa M (2012) Fractal analysis of ULF electromagnetic emissions in possible association with earthquakes in China, Nonlin. Process Geophys 19:577–583. https://doi.org/10.5194/npg-19-577-2012
Jin A, Aki K (1986) Temporal change in coda Q before the Tangshan Earthquake of 1976 and the Haicheng Earthquake of 1975. J Geophy Res Solid Earth. https://doi.org/10.1029/JB091iB01p00665
Johnston MJS, Smith BE, Johnson JR, Williams FJ (1973) A search for tectonomagnetic effects in California and western Nevada. In: Kovach RL, Nur A (eds) Proceedings of conference on tectonic problems of the San Andreas Fault System. Stanford University Press, pp 225–239

Johnston MJS, Mueller RJ, Ware RH, Davis PM (1984) Precision of geomagnetic measurements in a tectonically active region. J Geomagn Geoelectr 36:83–95

Jordan TH, Chen YT, Gasparini P, Madariaga R, Main I, Marzocchi W, Papadopoulos G, Sobolev G, Yamaoka K, Zschau J (2011) Operational earthquake forecasting: state of knowledge and guidelines for utilization. Report by the International Commission on Earthquake Forecasting for Civil Protection

Kanamori H, Brodsky EE (2001) The physics of earthquakes. Phys Today 54:34–40

Karakelian D, Klemperer SL, Fraser-Smith AC, Beroza GC (2000) A transportable system for monitoring ultra lowfrequency electromagnetic signals associated with earthquakes. Seismol Res Lett 71(4):423–436

Kapiris P, Eftaxias K, Nomikos K, Polygiannakis J, Dologlou E et al (2003) Evolving towards a critical point: a possible electromagnetic way in which the critical regime is reached as the rupture approaches. Nonlinear Process Geophys 10:511–524

Kapiris PG, Eftaxias KA, Chelidze TL (2004) Electromagnetic signature of prefracture criticality in heterogeneous media. Phys Rev Lett 92(6):065702. https://doi.org/10.1103/PhysRevLett.92.065702

Kawate R, Molchanov OA, Hayakawa M (1998) Ultra-low frequency magnetic fields during the Guam earthquake of 8 August 1993 and their interpretation. Phys Earth Planet Inter 105:229–238

Koizumi N, Kitagawa Y, Matsumoto N, Takahashi M, Sato T, Kamigai O, Nakamura K (2004) Preseismic groundwater level changes induced by crustal deformations related to earthquake swarms off the east coast of Izu Peninsula, Japan. Geophys Res Lett. https://doi.org/10.1029/2004GL019557

Kopytenko Yu A, Matiashvili TG, Voronov PM, Kopytenko EA, Molchanov OA (1993) Detection of ultra-low-frequency emissions connected with the Spitak earthquake and its aftershock activity, based on geomagnetic pulsations data at Dusheti and Vardzia observatories. Phys Earth Planet Inter 77(1–2):85–95. ISSN 0031-9201. https://doi.org/10.1016/0031-9201(93)90035-8

Korepanov V, Hayakawa M, Yampolski Y, Lizunov G (2009) AGW as a seismo-ionospheric coupling responsible agent. Phys Chem Earth 34:485–495. https://doi.org/10.1016/j.pce.2008.07.014

Liu JY, Chen CH, Chen YI, Yen HY, Hattori K, Yumoto K (2006) Seismo-geomagnetic anomalies and M P 5.0 earthquakes observed in Taiwan during 1988–2001. Phys Chem Earth 31(2006):215–222. https://doi.org/10.1016/j.pce.2006.02.009

Lu X, Meng QY, Gu XF, Zhang XD, Xie T, Geng F (2016) Thermal infrared anomalies associated with multi-year earthquakes in the Tibet region based on China's FY-2E satellite data. Adv Space Res. 58(6):989–1001. https://doi.org/10.1016/j.asr.2016.05.038

Main I (1999) Long odds on prediction. Nature 385:19–20

Main IG, Bell AF, Meredith PG, Geiger S, Touati S (2012) The dilatancy-diffusion hypothesis and earthquake predictability. Geol Soc Lond Spec Publ 367(1):215–230. https://doi.org/10.1144/SP367.15

Martinelli G, Facca G, Genzano N, Gherardi F, Lisi M, Pierotti L et al (2020) Earthquake-related signals in Central Italy detected by hydrogeochemical and satellite techniques. Front Earth Sci 8:529. https://doi.org/10.3389/feart.2020.584716

Masci F, Di Persio M (2012) Retrospective investigation of geomagnetic field time-series during the 2009 L'Aquila seismic sequence. Tectonophysics 530–531:310–317. https://doi.org/10.1016/j.tecto.2012.01.008

Masci F, Thomas JN (2013a) Comment on "Fractal analysis of ULF electromagnetic emissions in possible association with earthquakes in China" by Ida et al. (2012). Nonlinear Process Geophys 20:417–421. https://doi.org/10.5914/npg/20-/417/2013a

Masci F, Thomas JN (2013b) Review Article: on the relation between the seismic activity and the Hurst exponent of the geomagnetic field at the time of the 2000 Izu swarm. Nat Hazards Earth Syst Sci 13:2189–2194. https://doi.org/10.5194/nhess-13-2189-2013

Masci F, Thomas JN (2015a) Are there new findings in the search for ULF magnetic precursors to earthquakes? J Geophys Res Space Phys 120:10289–10304. https://doi.org/10.1002/2015JA021336

Masci F, Thomas JN (2015b) On the reliability of the Spatial Scintillation Index to detect earthquake precursors in the ionosphere. Radio Sci 50:745–753. https://doi.org/10.1002/2015RS005734

Matthews RAJ (1997) Decision-theoretic limits on earthquake prediction. Geophys J Int 131(3):526–529. https://doi.org/10.1111/j.1365-246X.1997.tb06596.x

Minadakis G, Potirakis S, Nomicos C, Eftaxias K (2012) Linking electromagnetic precursors with earthquake dynamics: an approach based on non-extensive fragment and self-affine asperity models. Physica A 391:2232–2244

Molchanov OA, Hayakawa M (1998) On the generation mechanism of ULF seismogenic electromagnetic emissions. Phys Earth Planet Inter 105:201–210

Molchanov OA, Kopytenko YA, Voronov PM, Kopytenko EA, Matiashvily TG, Fraser-Smith AC, Bernardi A (1992) Results of ULF magnetic field measurements near the epicenters of the Spitak

(Ms = 6, 9) and Loma Prieta (Ms = 7, 1) earthquakes: comparative analysis. Geophys Res Lett 19(14):1495–1498
Molchanov O, Fedorov E, Schekotov A, Gordeev E, Chebrov V, Surkov V et al (2004a) Lithosphere–atmosphere–ionosphere coupling as governing mechanism for preseismic short-term events in atmosphere and ionosphere. Nat Hazards Earth Syst Sci 4(5–6):757–767. https://doi.org/10.5194/nhess-4-757-2004
Molchanov OA, Schekotov A Yu, Fedorov E, Belyaev GN, Solovieva MS, Hayakawa M (2004b) Preseismic ULF effect and possible interpretation. Ann Geophys 47:119–131
Nagao T, Enomoto Y, Fujinawa Y, Hata M, Hayakawa M, Huang Q, Izutsu J, Kushida Y, Maeda K, Oike K, Uyeda S, Yoshino T (2002) Electromagnetic anomalies associated with 1995 Kobe earthquake. J Geodyn 33:401–411. https://doi.org/10.1016/S0264-3707(02)00004-2
Nakatani M (2020) Evaluation of phenomena preceding earthquakes and earthquake predictability. J Disaster Res. https://doi.org/10.20965/jdr.2020.p0112
Nikolaeva NA, Derkachev AN, Obzhirov AI (2009) Characteristic features of the occurrence of gas-fluid emanations on the northeastern slope of Sakhalin Island, sea of Okhotsk. Russ J Pac Geol 3 (3):234–248. https://doi.org/10.1134/S181971400903004X
Ouzounov D, Liu D, Chunli K, Cervone G, Kafatos M, Taylor P (2007) Outgoing long wave radiation variability from IR SatelliteData prior to major earthquakes. Tectonophysics 431(1–4):211–220. https://doi.org/10.1016/j.tecto.2006.05.042
Ouzounov D, Pulinets S, Hattori K, Taylor P (2018) Pre-earthquake processes: a multidisciplinary approach to earthquake prediction studies, 384 pp. ISBN: 978-1-119-15695-6
Panda SK, Choudhury S, Saraf AK, Das JD (2007) MODIS land surface temperature data detects thermal anomaly preceding 8 October 2005 Kashmir Earthquake. Int J Remote Sens 28(20):4587–4596. https://doi.org/10.1080/01431160701244906
Park SK (1996) Precursors to earthquakes: seismoelectromagnetic signals. Surv Geophys 17(493–516):1996
Park SK, Johnston MJS, Madden TR, Morgan FD, Morrison HF (1993) Electromagnetic precursors to earthquakes in the Ulf band: a review of observations and mechanisms. Rev Geophys 31(2):117–132. https://doi.org/10.1029/93RG00820
Petraki E, Nikolopoulos D, Chaldeos Y, Coulouras G, Nomicos C, Yannakopoulos PH, Kottou S, Stonham J (2016) Fractal evolution of MHz electromagnetic signals prior to earthquakes: results collected in Greece during 2009. Geomat Nat Haz Risk 7(2):550–564. https://doi.org/10.1080/19475705.2014.945496
Pham VN, Geller RJ (2002) Comment on '"Signature of pending earthquake from electromagnetic anomalies"' by K. Eftaxias et al. Geophys Res Lett 29(18):1871. https://doi.org/10.1029/2002gl015328
Pham V-N, Boyer D, Chouliaras G, Savvaidis A, Stavrakakis G, Le Mouël J-L (2002) Sources of anomalous transient electric signals (ATESs) in the ULF band in the Lamia region (central Greece): electrochemical mechanisms for their generation. Phys Earth Planet Inter 130:209–233
Picozza P, Conti L, Sotgiu A (2021) Looking for earthquake precursors from space: a critical review. Front Earth Sci 9:676775. https://doi.org/10.3389/feart.2021.676775
Potirakis S, Minadakis G, Eftaxias K (2012) Analysis of electromagnetic pre- seismic emissions using Fisher information and Tsallis entropy. Physica A 391:300–306
Pulinets S, Boyarchuk K (2005) Ionospheric precursors of earthquakes. Springer, Berlin, Heidelberg. https://doi.org/10.1007/b137616
Pulinets S, Ouzounov D (2011) Lithosphere–atmosphere–ionosphere coupling (LAIC) model—an unified concept for earthquake precursors validation. J Asian Earth Sci 41(4–5):371–382. https://doi.org/10.1016/j.jseaes.2010.03.005
Rikitake T (1969) An approach to prediction of magnitude and occurrence time of earthquakes. Tectonophysics 8(2):81–95
Rikitake T (1975) Dilatancy model and Empirical formulas for an earthquake area. Pageoph 19:141–147
Samrock F, Kuvshinov A (2013) Tippers at island observatories: can we use them to probe electrical conductivity of the Earth's crust and upper mantle? Geophys Res Lett 40:824–828. https://doi.org/10.1002/grl.50218
Samuelson J, Elsworth D, Marone C (2009) Shear-induced dilatancy of fluid-saturated faults: experiment and theory. J Geophys Res 114:B12404. https://doi.org/10.1029/2008JB006273
Schekotov A, Fedorov E, Molchanov OA, Hayakawa M (2013) Low frequency electromagnetic precursors as a prospect for earthquake prediction. In: Hayakawa M (ed) Earthquake prediction studies: seismo electromagnetics, pp 81–99. TERRAPUB
Scholz CH, Sykes LR, Aggarwal YP (1973) Earthquake prediction: a physical basis. Science 181:4102
Scoville JH, Freund F (2015) Pre-earthquake magnetic pulses Nat. Hazards Earth Syst Sci 15:1873–1880. https://doi.org/10.5194/nhess-15-1873-2015

Sevgi L (2007) A critical review on electromagnetic precursors and earthquake prediction. Turk J Electr Eng Comput Sci 15:1–15

Sorokin V, Hayakawa M (2014) Plasma and electromagnetic effects caused by the seismic-related disturbances of electric current in the global circuit. Mod Appl Sci 8(4):61–83. https://doi.org/10.5539/mas.v8n4p61

Sorokin VM, Chmyrev VM, Hayakawa M (2020) A review on electrodynamic influence of atmospheric processes to the ionosphere. Open J Earthq Res 09(02):113–141. https://doi.org/10.4236/ojer.2020.92008

Storchak DA, Bird AL, Adams RD (2000) Discrepancies in earthquake location between ISC and other agencies. J Seismolog 4:321–331

Szakács A (2021) Precursor-based earthquake prediction research: proposal for a paradigm shifting strategy. Front Earth Sci 8:548398. https://doi.org/10.3389/feart.2020.548398

Takla EM, Khashaba A, Abdel Zaher M, Yoshikawa A, Uozumi T (2018) Anomalous ultra low frequency signals possibly linked with seismic T activities in Sumatra, Indonesia. NRIAG J Astron Geophys 7:247–252. https://doi.org/10.1016/j.nrjag.2018.04.004

Tanaka S, Ohtake M, Sato H (2002) Spatio-temporal variation of the tidal triggering effect on earthquake occurrence associated with the 1982 South Tonga Earthquake of Mw 7.5. Geophys Res Lett 29(16):3-1–3-4. https://doi.org/10.1029/2002gl015386

Thanassoulas C, Klentos V, Verveniotis G (2008) On a preseismic electric field “strange attractor” like precursor observed short before large earthquakes (arXiv preprint)

Uyeda S, Nagao T (2018) International cooperation in pre-earthquake studies: history and new directions. In: Ouzounov D, Pulinets S, Hattori K, Taylor P (eds) Geophysical monograph series. Wiley publications. https://doi.org/10.1002/9781119156949.ch1

Varotsos P, Al Exopoulos K (1984a) Physical-properties of the variations of the electric-field of the earth preceding earthquakes. 1. Tectonophysics 110(1–2):73–98

Varotsos P, Al Exopoulos K (1984b) Physical-properties of the variations of the electric-field of the earth preceding earthquakes 2. Determination of epicenter and magnitude. Tectonophysics 110(1–2):99–125

Varotsos P, Alexopoulos K (1986) Stimulated current emission in the Earth: piezostimulated currents and related geophysical aspects. In: Thermodynamics of point defects and the relation with bulk properties. Elsevier, New York, pp 410–412, 417–420

Virk HS, Walia V, Kumar N (2001) Helium/radon precursory anomalies of Chamoli Earthquake, Garhwal Himalaya. India J Geodyn 31(2):201–210. https://doi.org/10.1016/S0264-3707(00)00022-3

Wang K, Chen QF, Sun S, Wang A (2006) Predicting the 1975 Haicheng earthquake. Bull Seismol Soc Am 96:757e795. https://doi.org/10.1785/0120050191

Wang C, Christman LE, Klemperer SL, Glen JM, McPhee DK, Chen B (2022) Assessment of a claimed ultra-low frequency electromagnetic (ULFEM) earthquake precursor. Geophys J Int 229:2081–2095. https://doi.org/10.1093/gji/ggab530

Warwick JW, Stoker C, Meyer TR (1982) Radio emission associated with rock fracture: possible application to the Great Chilean Earthquake of May 22, 1960. J Geophys Res 87(B4):2851–2859. https://doi.org/10.1029/JB087iB04p02851

Wyss M (1997) Cannot earthquakes be predicted? Science 278:487–490

Wyss M (2001) Why is earthquake prediction research not progressing faster? Tectonophysics 338(3–4):217–223. https://doi.org/10.1016/S0040-1951(01)00077-4

Wyss M, Allmann A (1996) Probability of chance correlations of earthquakes with predictions in areas of heterogeneous seismicity rate: the VAN case. GRL 23(11):1307–1310

Yasuoka Y, Igarashi G, Ishikawa T, Tokonami S, Shinogi M (2006) Evidence of precursor phenomena in the Kobe earthquake obtained from atmospheric radon concentration. Appl Geochem 21(6):1064–1072. https://doi.org/10.1016/j.apgeochem.2006.02.019

Yumoto K et al (2009) A new ULF wave analysis for seismo-electromagnetics using CPMN/MAGDAS data. Phys Chem Earth 34:360–366

Zhao Y, Qian F (1994) Geoelectric precursors to strong earthquakes in China. Tectonophysics 233(1–2):99–113. https://doi.org/10.1016/0040-1951(94)90223-2

Zhao Y, Qian F, Xu T (1991) The relationship between resistivity variation and strain in a load-bearing rock-soil layer. Acta Seismoh Sin 4:127–137